Design and Control of Close Proximity Indirect Exposure for Nonthermal Atmospheric Pressure Plasma-Based Oxidation of Carbon Fiber Precursor

A Dissertation Presented for the

Doctor of Philosophy

Degree

The University of Tennessee, Knoxville

Truman Andrew Bonds

December 2016

DEDICATION

This work is dedicated to:

My Father in Heaven who set me on this path before I was born and carried me through it,

My wife Caitlin, for her incredible love, patience and support,

My children, Hannah, Solomon and Adah for dealing with my frequent absence,

My parents Richard and Sandra who encouraged me to persevere.

ACKNOWLEDGEMENTS

I would like to express my deep gratitude to my advisor Prof. Seddik Djouadi at the University of Tennessee for his patience and flexibility in supporting my research efforts and in pursuing this PhD. I would like to thank Dr.-Eng. Felix Paulauskas at the Oak Ridge National Laboratory for his willingness to give an upstart engineer a shot at taking on the plasma engineering role on his projects over 10 years ago, and his strong support through the conclusion of my work and defense of my dissertation. A very special thanks to Rod Grubb, Dick Nixdorf and Doug Mentzer for helping me start RMX Technologies in 2011 to take the early research to the next level. I would like to thank RMX for its financial support both in conducting the research and funding my tuition. Thank you to RMX staff that helped support this work over the years including Corey Bounds, Dr. Jeremy Jackson (deceased), David Martin, Pol Grappe, Rob Fogg, Jonathan Ford and Nick Grubb.

I would like to express my appreciation to the U.S. Department of Energy's Vehicle Technologies Office for funding the majority of this work, and to the Oak Ridge National Laboratory, for their partnership on this effort.

ABSTRACT

A new plasma-based method for the stabilization of polyacrylonitrile carbon fiber precursor utilizing reactive chemical species derived from a custom atmospheric pressure plasma generation system was developed and demonstrated. As opposed to the conventional stabilization method of convective heating in air, plasma-based stabilization efficiently introduces oxidative reactive species that both diffuse through and react faster with the precursor filaments, resulting in a faster and more efficient process. This method was successfully demonstrated with a variety of precursor chemistries, grades and sizes. The development effort was entirely experimental, with successive processing devices designed and constructed to examine various aspects of the process and to scale the technique to ever-greater throughput. The technology was scaled from the benchtop level to the small pilot line scale of 1 annual metric tons of throughput. The author was directly responsible for inventing a new plasma processing method, developing the theory behind it, designing and implementing the plasma generation system, and integrating it with the experimental processing equipment. Compared to conventional oxidation, plasma oxidation has demonstrated a 2.5-3X reduction in processing time with a 75% reduction in unit energy savings, all while meeting or exceeding the final fiber properties from conventional processing.

TABLE OF CONTENTS

LIST OF TABLES

LIST OF FIGURES

ABBREVIATIONS

LTE	Local Thermodynamic Equilibrium
DBD	Dielectric Barrier Discharge
MPC	Model Predictive Control
RE	Remote Exposure
DE	Direct Exposure
CPIE	Close Proximity Indirect Exposure
EHD	Electrohydrodynamic
SMR2	Surface Modification Reactor 2
STR1	Single Tow Reactor 1
STR2	Single Tow Reactor 2
MTR1	Multiple Tow Reactor 1
MTR2	Multiple Tow Reactor 2

CHAPTER 1: INTRODUCTION

1.1 Plasma Physics

There are four common states of ordinary visible matter in our universe: solid, liquid, gas and plasma. The addition of sufficient energy into a given state will transform it into the next state in order – solid to liquid to gas to plasma [1]. The plasma state accounts for more than 99% of the total existence of these states in the universe, but is not very common on earth [2]. Examples of natural plasma on earth include lightning and the Aurora Borealis [1]. Plasma physics play an important role on earth in terms of weather, and, in the last 100 years, have increasingly played a vital role in manmade industrial applications [3]. Materials processing applications are by far the most common application, with computer chip fabrication being one example. Plasma discharges present two unique advantages for materials processing applications: They offer greater temperatures and energy densities than that which can be achieved by other means, and they can produce active species that can yield results that cannot be achieved by other means [3]. This dissertation will present a new development in one such materials processing application for plasma, namely the plasma-based oxidation of carbon fiber precursors.

1.2 Oxidation Chemistry

The process of oxidation is a common occurrence in nature, and plays an important role in materials science and the products we commonly use today. Oxidation plays a role in making materials more stable and resistant from chemical and thermal degradation. This is one reason why most metals found in nature are in their oxidized state. Oxidation is also a critical processing step for many advanced materials.

1.3 Carbon Fiber Manufacturing

A specific example of this is examined in this work, and is an important step in the manufacture of carbon fiber. Over 96% of the world's carbon fiber comes from acrylic, a common product refined from oil [4]. The acrylic feedstock, typically in powder form, is first polymerized and spun into continuous filament fiber form called polyacrylonitrile (PAN) and then converted through a series of processing steps into carbon fiber, being over 99% pure carbon [5]. This process is illustrated in Figure 1.

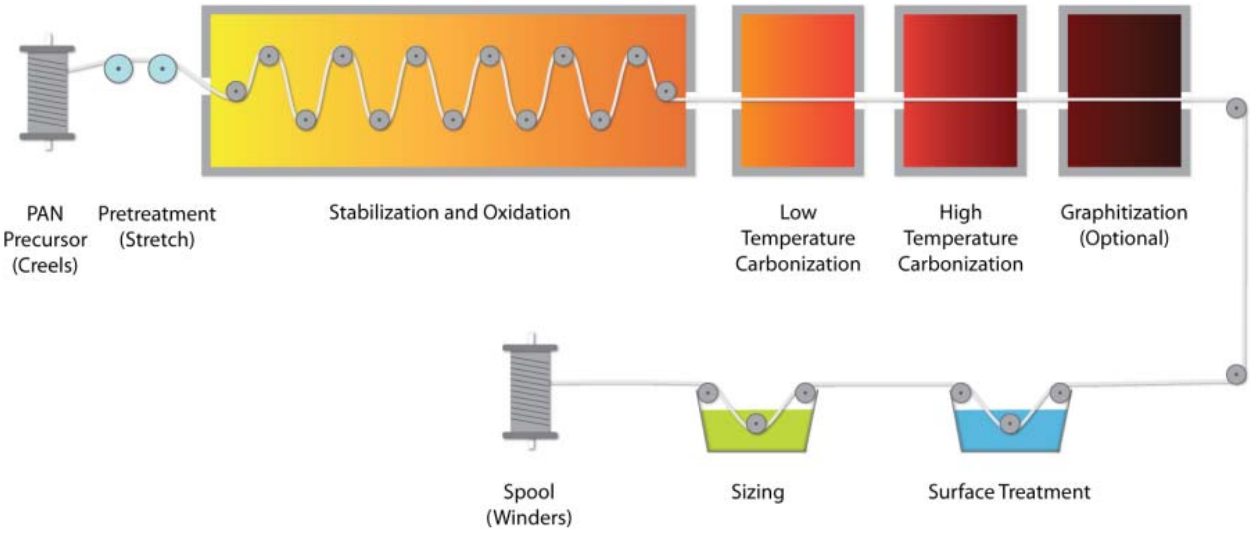

Figure 1: The conventional conversion process for turning polyacrylonitrile precursor into carbon fiber [6]**.**

The above steps are outlined below with key facts coming from [5].

1. PAN Precursor: PAN is manufactured and spun onto spools or folded in a box for storage and shipment to a conversion plant. Individual bundles of fiber are called tows, and each tow usually contains anywhere from 1500 to over 300,000 filaments. Typically, the smaller the tow, the better the quality and resulting carbon fiber mechanical properties.
2. Pretreatment: This is an optional step where the precursor may be stretched in a steam stretcher to improve the molecular alignment of the individual filaments. Some chemical pretreatment may be performed as well.

3. Stabilization and Oxidation: This is the step of interest for the body of work presented in this document. In this step a series of reactions are induced through a combination of convective thermal treatment and fiber stretching. Coming out of this step, the fiber is chemically and thermally stabilized (being converted from a thermoplastic to a thermoset) and will be ready to survive the next steps of carbonization. The temperatures involved are typically from 180 – 300 ºC. The equipment utilized is commonly called an oxidation oven.
4. Low Temperature Carbonization: The first step of carbonization where the majority of the chemical content that is not carbon is burned off. Since polyacrylonitrile is only 50-55% carbon, it loses 45-52 % of its mass during this stage. Usually, a dedicated furnace capable of producing temperatures up to and over 600 ºC is used in this step.
5. High Temperature Carbonization: The final required step of carbonization that finalizes the structure of the fiber into true carbon fiber. A second dedicated furnace with temperatures up to 1500 ºC is used in this step.
6. Graphitization: This optional step enhances the crystallinity of the carbon fiber to further increase its stiffness. This step adds considerable expense to the final products so is only used in high-end aerospace applications. A third dedicated furnace with temperatures up to 2500 ºC or more is used.
7. Surface Treatment: This is an essential step that contributes to the mechanical properties of the carbon fiber part (fiber plus resin). The individual carbon fiber filaments are chemically inert and do not bond well with resins, so a chemical treatment, typically a wet electrolysis bath process, is performed to improve the fiber bond to sizings and resins.
8. Sizing: A polymer coating is applied to the final carbon fiber product to protect the fiber and improve its handling, preserve the surface treatment, and further enhance its bonding to the subsequent resin used in part fabrication.
9. Spooling/Packaging: After manufacture, the fiber is spooled or bundled in a box for shipping to a carbon fiber part fabricator.

With this summary of the carbon fiber manufacturing process in mind, the focus now turns to the oxidation step. This step has traditionally been the bottleneck of the entire process due to the required long processing times – typically 80-120 minutes. Any method of cutting this processing time in half or more would dramatically improve the cost economics of the carbon fiber market. This was the impetus for an investigation that led to the development of a plasma-based oxidation process that now has been successfully demonstrated to reduce the oxidation time by 3X – down to 20-30 minutes.

1.4 Dissertation Outline

In Chapter 2, prior art is presented related to plasma science, and industrial plasma applications related to plasma modeling, control of plasma, and materials processing. Prior art work related to the oxidation process of PAN precursor is also discussed.

In Chapter 3, prior work on plasma oxidation, before this author's involvement, is briefly presented.

In Chapter 4, the theory and method of plasma-based oxidative stabilization of carbon fiber precursor is presented. Differentiation between various plasma exposure techniques and the impetus behind them leading to the design, fabrication, control and modification of different experimental equipment utilized for this work.

In Chapter 5, the methods and implementation of control techniques are presented. Both the hardware and software utilized are discussed. Power matching schemes were utilized to optimize power transferred to the plasma.

In Chapter 6, hardware development under the direction of this author is presented. Scaling is a focus of the work, and progress from proof of principal concept to the 1 aMT oven is presented.

In Chapter 7, the resulting impact of the plasma-based process on the fiber is discussed. Two different experimental setups are utilized and the results contrasted.

In Chapter 8, final conclusions are presented and future work is outlined.

CHAPTER 2: PRIOR ART

2.1 Plasma Science

The term plasma was first defined by Irving Langmuir in 1928 as an approximately electrically neutral collection of ions and electrons, which may or may not contain a background neutral gas, and that respond to electric and/or magnetic fields [3]. Industrial plasmas are those that are generated from manmade industrial devices, processes, or products that utilize the plasma [3]. There are several different ways to categorize industrial plasmas, depending on one's point of view. Industrial plasmas can be categorized by how they are generated, coupling mechanisms, their discharge physics, the environment in which they exist, or by their end application. An example of categorization by discharge physics would be as follows: glow discharges, arc discharge, atmospheric pressure discharges, high frequency discharges, aerosol and dusty plasmas, and electron beam plasmas [1]. Within atmospheric pressure discharges, two general categories exist based on the thermodynamic state of the plasma species, namely, thermal (hot) and nonthermal (cold). The differences in these two regimes lies in the thermal state of the ions and any neutrals found within a plasma volume. In a thermal plasma, all three main species, the electrons, ions, and neutrals, are generally at the same temperature, i.e. local thermodynamic equilibrium (LTE). In a nonthermal discharge, they are not at LTE, and the most common arrangement is that the electrons are hot, while the ions and neutrals are at near room temperature. *How hot* depends on several factors including the amount of energy coupled to the plasma, but typically can approach 20,000 K (several eV in temperature) or more. This type, the atmospheric pressure discharge, is the method utilized in this work. Within this category, one will find plasma discharges such as coronas, dielectric barrier discharges (DBD), and sparks. The dielectric barrier discharge is the general design approach to this work and will be discussed briefly.

A common parameter that is critical to proper plasma ignition is the breakdown voltage. This voltage must be exceeded to ignite a plasma in any neutral gas, and is the voltage at which the gas can no longer resist current flow with its electrical insulative properties. For dry air at standard temperature and pressure, this value is given by [3]:

$$V_B = 3000d + 1.35 \text{ [kV]} \quad (1)$$

where d is the distance between the two electrodes in meters.

In fact, the breakdown voltage for a given gas is only a function of pressure times the distance between electrodes. This fact is known as Paschen's law [3]. A related parameter is the ionization potential of a given gas. This is a measure of how much energy an electron needs to ionize a molecule of the gas. Most atmospheric pressure nonthermal discharges are only partially ionized, which means a significant percentage of the species inside the plasma volume are neutral species. This is true for the current application with plasma oxidation.

The dielectric barrier discharge was first invented in 1857 by Werner von Siemens [7] and is shown in Figure 2. The unique aspect of this plasma generation method was that the conducting electrodes were not in direct contact with the plasma, which created certain advantages over previous methods. This method was useful for chemical reaction generation, but was typically highly filamentary at atmospheric pressure, i.e. more or less a collection of filaments or microdischarges.

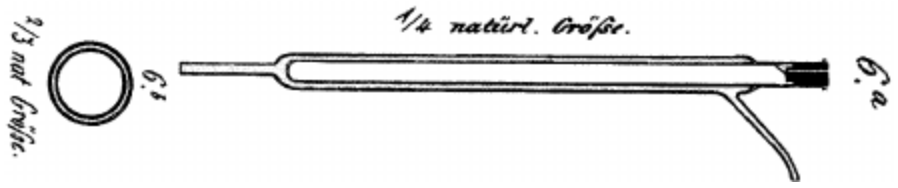

Figure 2: Invention of the dielectric barrier discharge by Werner von Siemens in 1857 [7].

It was not until the 1960s when it was discovered that atmospheric pressure diffuse discharges were possible with tightly controlled conditions [8]. The term “diffuse” captures two scenarios of discharge physics: a) the microdischarges are so closely packed and uniformly distributed that the net processing effect is generally uniform, and b) a truly homogeneous discharge volume similar to low pressure discharges. To the naked eye, these two scenarios will appear similar, but the physics and mechanisms of breakdown are very different. It is extremely difficult to produce a truly homogenous plasma volume in the presence of oxygen [8]. Since the presence of oxygen is required in this work, it is this first type of diffuse discharge that is utilized. The typical modern arrangement of a parallel-plate dielectric barrier discharge is shown in Figure 3 below.

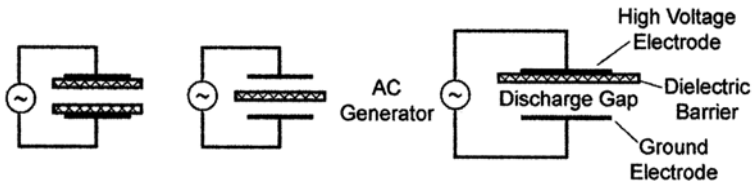

Figure 3: Common configurations for a dielectric barrier discharge [7].

As can be concluded by the name, the key feature of a DBD is its dielectric barrier. The material properties and geometric aspects strongly influence the resulting plasma properties. An alternative configuration, invented at the University of Tennessee in the late 1990s, is the surface-layer dielectric barrier discharge, shown in Figure 4. It was soon found that a slight modification of this arrangement, illustrated in Figure 5, results in mechanical flow inducement of the surrounding neutral gas. The result is essentially an electric fan with no moving parts.

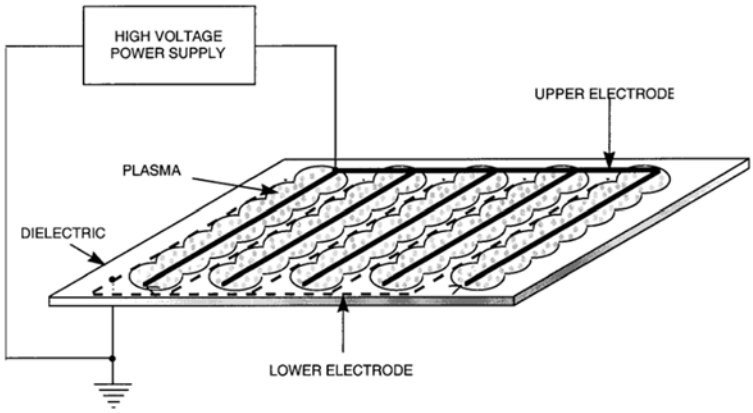

Figure 4: An illustration of the surface-layer dielectric barrier discharge [9].

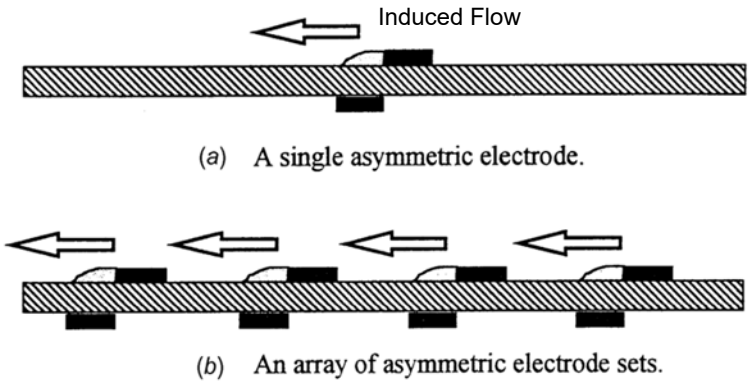

Figure 5: A surface-layer dielectric barrier discharge that induces flow in the surrounding gas illustrated by the arrows [9].

It is the fundamental aspects of a surface-layer dielectric barrier discharge in a diffuse filamentary mode of operation that is the basis for the present application. There is no other prior work in the literature that this author is aware of that takes advantage of the unique characteristics of this type of discharge. Advances in both configuration and materials selection originated by the author in the final implementation are discussed in the next chapter.

Industrial plasma technology is useful in that it can induce a unique set of chemical reactions between the ions, electrons, and neutral species. The most common types of reactions that occur in a plasma are summarized in Table 1. The definitions are:

- The $^{+}$ and $^{-}$ symbols denote electric charge
- The * symbol denotes an excited state
- *h v* denotes photon emission energy (Plank's constant times frequency)
- A, B, C denote atomic or molecular species

In the types of plasma used in this work, the nonthermal (or nonequilibrium) type previously mentioned, the primary reaction initiation mechanism is through the electrons [10]. Electrons are energized by strong electric fields and in turn collide and react with the background neutral species. These collisions lead to the types of reactions shown below. Because of the complexity of modern plasma technology, focus has turned to numerical modeling and simulation to approximate and predict plasma behavior.

Table 1: Common reactions that occur in a plasma [3].

Electrons	
$e + A \rightarrow A^+ + 2e$	Ionization
$e + A \rightarrow e + A^* \rightarrow e + A + h\nu$	Excitation
$e + A^* + B \rightarrow 2e + A + B^+$	Penning ionization
$e + A \rightarrow e + A$	Elastic scattering
$e + AB \rightarrow e + A + B$	Dissociation
$e + AB \rightarrow 2e + A^+ + B$	Dissociative ionization
$e + AB \rightarrow A^- + B$	Dissociative attachment
$e + A^+ + B \rightarrow A + B$	Recombination
Ions	
$A^+ + B \rightarrow A + B^+$	Charge exchange
$A^+ + B \rightarrow A^+ + B$	Elastic scattering
$A^+ + B \rightarrow A^+ + B^+ + e$	Ionization
$A^+ + B \rightarrow A^+ + B^* \rightarrow A^+ + B + h\nu$	Excitation
$A^+ + e + B \rightarrow A + B$	Recombination
$A^+ + BC \rightarrow A^+ + B + C$	Dissociation
$A + BC \rightarrow C + AB$	Chemical reaction

2.2 Modelling and Control of Plasma

Attempts to numerically model or simulate plasma physics goes back to the mid-1970s beginning with one-dimensional models [11]. Early work focused on thermal plasma discharges since, being at local thermodynamic equilibrium (LTE), they were much easier to model than nonthermal plasma. When physical regimes transition from LTE plasma to nonequilibrium plasma, the ability to accurately determine internal plasma parameters decreases.

2.2.1 Electrical Circuit Models

Electrical circuit models of plasma discharges that utilize sinusoidal excitation in the kHz frequency range can typically be framed within a lumped-element framework, since a plasma's largest dimension is much smaller than the wavelength of the excitation signal. Several models have been developed in the field for a variety of plasma systems. One such model is that by Orlov *et al.* [12]. Previous work by this group developed a generalized model as illustrated in Figure 6.

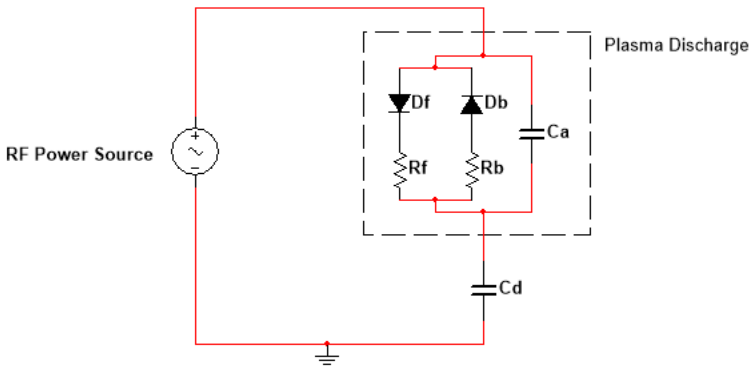

Figure 6: Generalized electrical circuit of a plasma actuator [12].

The individual components are defined as:

$$C_a = \frac{\varepsilon_0 \varepsilon_a A}{l} \quad (2)$$

$$R = \frac{\rho l}{A} \quad (3)$$

$$C_d = \frac{\varepsilon_0 \varepsilon_d A}{l} \quad (4)$$

where,

- D_f and D_b are diodes that represent the breakdown voltage trigger of a plasma discharge.
- R_f and R_b are the forward and reverse resistances of the plasma discharge. In the article, R is defined using the resistivity of air for ρ. However, this resistivity changes (drops) once the plasma is active, and this is not made clear in the article [12].
- C_a is the capacitance of the air gap between the two electrodes. The equation includes the relative permittivity of air, as well as the area and gap distance of the electrodes. This figure will also change once the plasma is active.
- C_d is the capacitance of the dielectric barrier. This value will remain constant during activation.

In the this paper [12], this group extrapolated their generalized form into spatial segments along the width-wise dimension of the plasma discharge, as shown in Figure 7. They were able to utilize this model to measure the impact of distance from the upper electrode edge on the voltage and current characteristics of the plasma. They confirmed the simulated circuit results with correlation to light emission detection using a photomultiplier tube.

Another group, led by Kurniawan *et al.* [13], utilized another electrical circuit to conduct simulation of a capacitively coupled plasma discharge. The goal of their work was to predict the effect of pressure on the electrical properties of the plasma. Their experimental setup is shown in Figure 8 below.

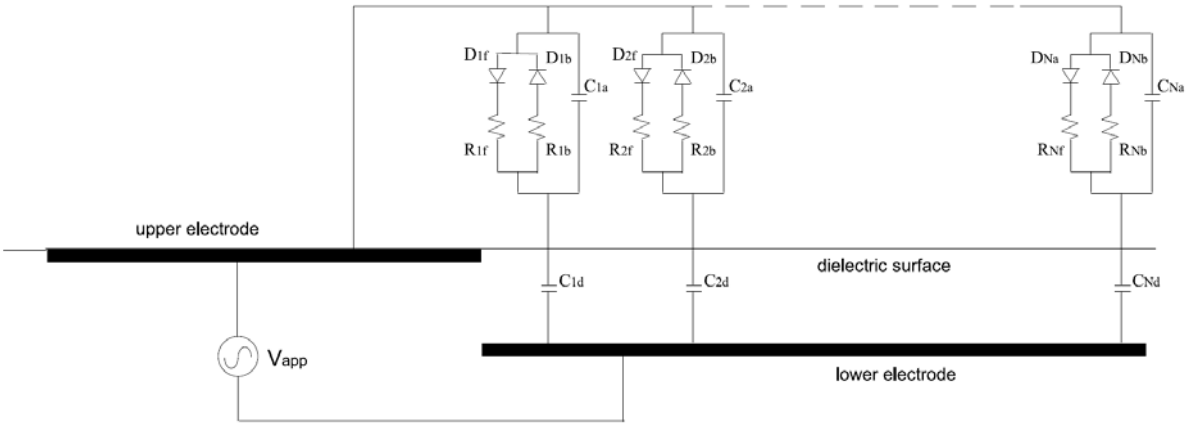

Figure 7: Spatially resolved electrical circuit of a plasma actuator [12].

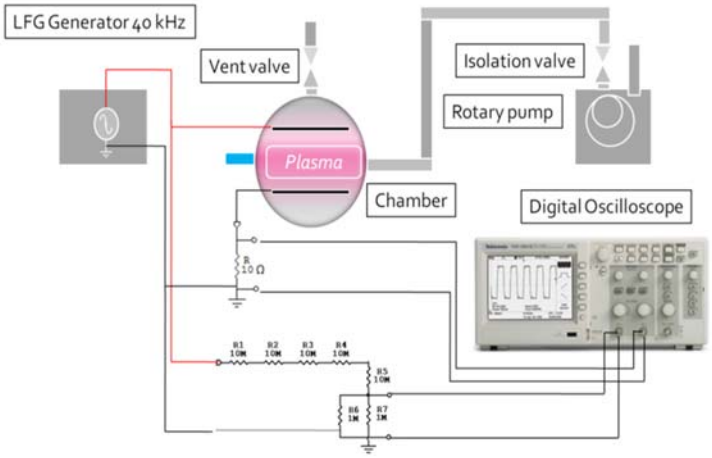

Figure 8: Experimental setup of Kurniawan [13].

The equivalent circuit model they utilized is shown in Figure 9. What is unique here is the group broke up the plasma discharge into three distinct segments for modeling (the three rows in the figure). Since this was a vacuum plasma, distinct plasma structures are present that do not exist at atmospheric pressure. The plasma has a physical regime close to the electrodes called sheaths. Sheaths are defined by the physics of the transition from the bulk plasma volume to the boundary conditions of the electrodes. As shown in this model, the sheath properties are different depending on whether they exist at the anode versus the cathode.

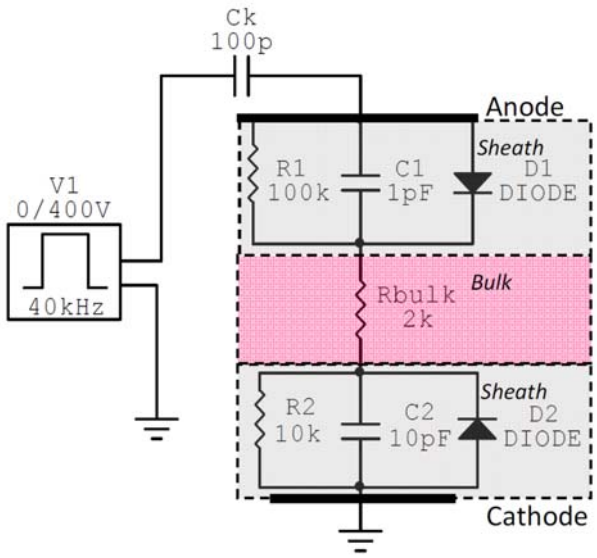

Figure 9: Circuit model of a capacitively coupled plasma discharge [13].

Yet another proposed equivalent circuit model is shown in Figure 10. A key difference in this approach is the use of a dependent current source (diamond shaped) to represent the dynamic current flow through the active plasma.

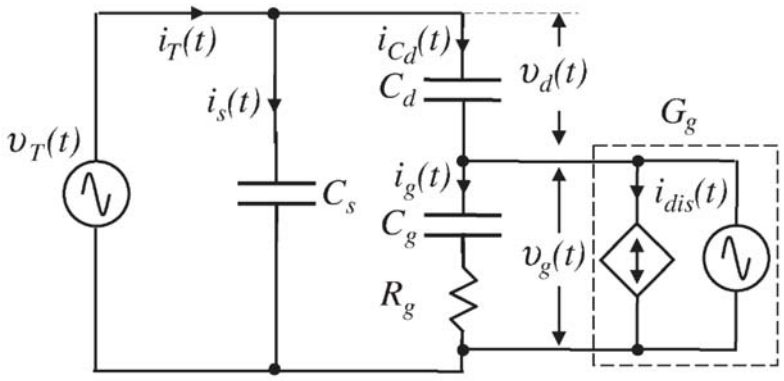

Figure 10: Circuit model of a parallel plate dielectric barrier plasma discharge [14].

The dependent current source that models the discharge current is defined as:

$$i_{dis}(t) = i_0(v_g(t)/V_b)^{\alpha} \quad (5)$$

where,

- i_0 is a gas dependent off-discharge value. In this work it ranged from 200 μA to 30 mA
- V_b is the breakdown voltage, which is gas and pressure dependent
- α is an exponent that ranges from 1 – 12 and is gas dependent

2.2.2 Plasma Kinetics

An excellent reference paper that discusses the fundamental kinetics of plasma discharges is found in Fridman et al [15]. In this paper, the Townsend and streamer breakdown mechanisms are presented, the latter of which is fundamental to the physics of a dielectric barrier discharge. The origin of the vast majority of electrical breakdowns is the electron avalanche. In free space everywhere there exist a very small concentration of free electrons generated by various background radiation sources (e.g. cosmic rays). In an industrial plasma discharge, with a sufficient electric or magnetic field strength, energy is imparted to one or more of these free electrons which begin to collide with neutral atoms or molecules, and knocking lose an electron from them. As energy continues to couple to the now two free electrons, they collide with other

neutral particles, and so on, creating an ever increasing avalanche of electrons until they collide with the anode or other conditions change. This is illustrated in Figure 11. In a dielectric barrier discharge, an electron avalanche leads to a streamer breakdown mechanism with typical timescales shown in Table 2. In Table 2, the third column describes the charge transferred from one electrode to the other.

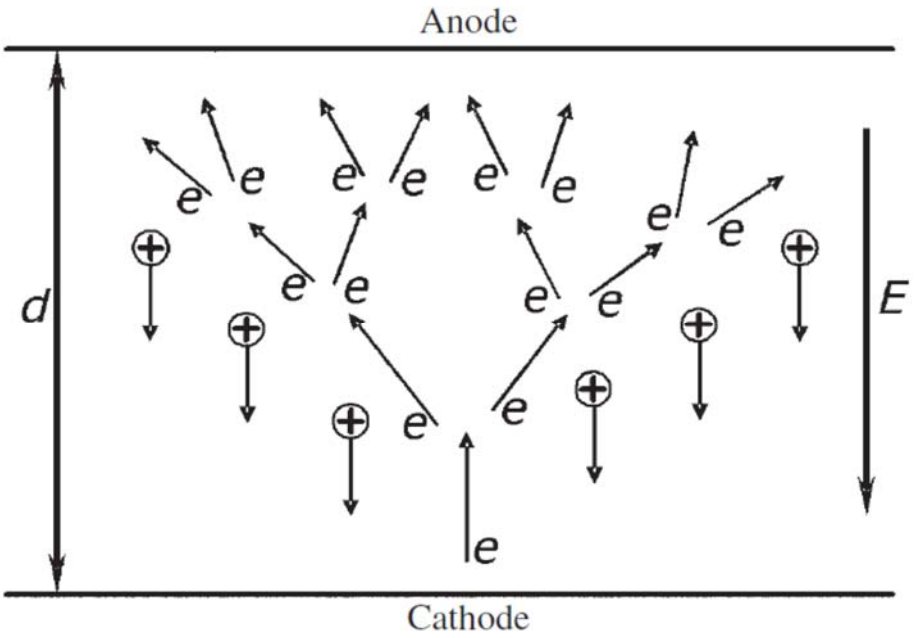

Figure 11: The electron avalanche [15].

Table 2: Timescales of a microdischarge [15].

	Duration	Charge Transferred
Microdischarge (0.2mm radius)	40 ns	10^{-9} C
-Electron Avalanche	10 ns	10^{-11} C
-Cathode-directed streamer	1 ns	10^{-10} C
-Plasma channel	30 ns	10^{-9} C
Microdischarge remnant	1 ms	$\geq 10^{-9}$ C

Distinct differences exist in the microdischarges of a dielectric barrier discharge versus classic streamer breakdown mechanisms. The main difference is in the effect the barrier has on the plasma discharge:

- The barrier prevents spark discharge of the streamer.
- The barrier allows for surface charge buildup from the space charge generated by the streamer.
- The barrier extinguishes the electron-based streamer, but slower moving ions remain for a bit longer.
- Unique patterns and filaments are created.

Typical parameters and values of a single microdischarge in a dielectric barrier discharge are listed in Table 3.

Table 3: Typical microdischarge parameters [15].

Lifetime	1-20 ns		Filament radius	50-100 μm
Peak current	0.1 A		Current density	0.1-1 kA cm^{-2}
Electron density	10^{14} - 10^{15} cm^{-3}		Electron energy	1-10 eV
Total transported charge	0.1 - 1 nC		Reduced electric field	$E/n = (1\text{-}2)(E/n)_{Paschen}$
Total dissipated energy	5 μJ		Gas temperature	Close to average, about 300K
Overheating	5 K			

A dielectric barrier discharge consists of thousands of microdischarges spread uniformly (if the electrode system is designed and implemented correctly) between the electrode surfaces. It is the cumulative effect of thousands of microdischarges per second that can produce significant change in the surrounding gas chemistry. With a surface barrier discharge, as is used in plasma oxidation, surface charge properties of the dielectric barrier can have significant influence on the overall physics of the plasma and resulting chemistry.

2.2.3 Control Methods for Plasma

Applying advanced control theory methodology to atmospheric pressure plasma has rarely been done. Most applications for this type of plasma operate in an open loop configuration not requiring active feedback control from the application itself (not considering any internal automatic power regulation in a plasma power supply). However, one such example can be found in a 2016 journal article by Gidon, et al [16]. This article actually claims to be "the first study on advanced control of cold atmospheric pressure devices." In their modeling work, they looked at controlling an atmospheric pressure plasma jet with a technique called model predictive control (MPC). The application was medical, and the control objective was to regulate the total thermal dosage of the plasma jet to the skin. This is illustrated in Figure 12 below.

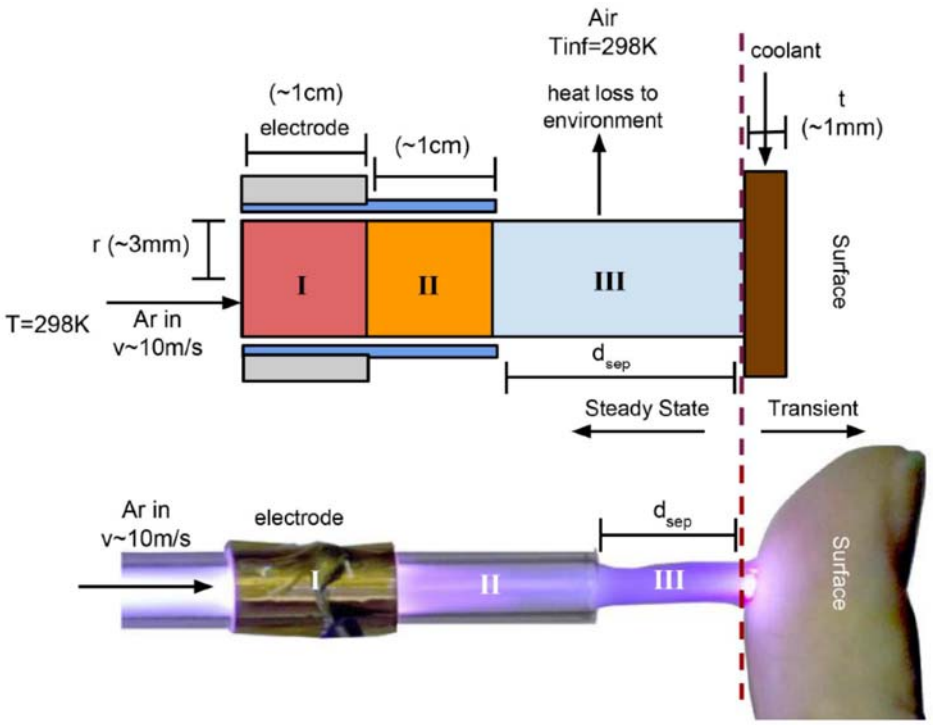

Figure 12: Schematic of an atmospheric pressure plasma jet for medical applications [16].

The regions I, II, and III are defined as follows:

- Region I contains the electrodes that ignite and sustain the plasma. The electrical phenomena and the formation of reactive and excited species mainly occur in this region. Thus, the majority of input power is dissipated here. The heat loss to the environment is negligible in this region due to the high heat transfer resistance of the tube wall.
- Region II represents the region along which the plasma discharge travels before extending to ambient air. The remaining input power is dissipated within this region. As in Region I, the heat loss is negligible.
- Region III is the afterglow region, in which there is no further energy deposition onto the gas. In this region, heat losses are large due to radial transport of heat to ambient air.

The control objective was to deliver a thermal dosage in region III on the skin surface without causing damage and honoring hardware constraints. The thermal dosage was reflected by a figure of merit called the cumulative equivalent minutes at 43 °C, or CEM_{43}. Skin damage occurs are CEM_{43} = 10 minutes. CEM_{43} is defined as:

$$CEM_{43} = \int_0^t K^{43-T_s} dt \tag{6}$$

Where,

$$f(x) = \begin{cases} 0, & T_s \leq 39℃ \\ 0.25, & 39℃ < T_s < 43℃ \\ 0.5, & T_s \geq 43℃ \end{cases} \tag{7}$$

T_s is the skin temperature

The control strategy was fairly basic. Utilize one sensory input, surface temperature, to feed the MPC control algorithm which control two outputs, plasma power and gas flow velocity. This is shown in Figure 13. The dosage must be delivered in 3-5 minutes.

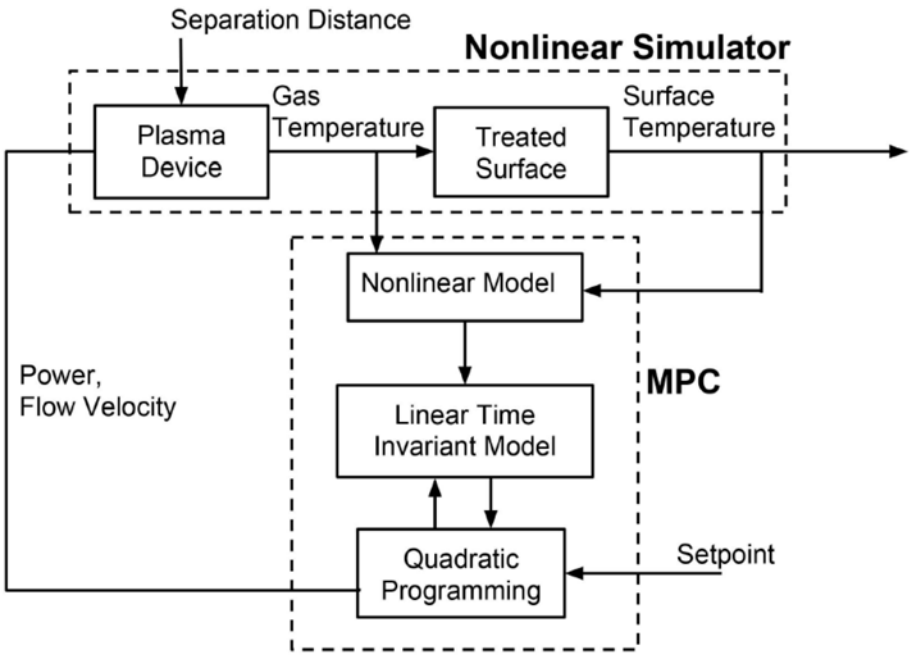

Figure 13: Block diagram of MPC control strategy [16].

Figure 14 shows the results of this control strategy in action. The target dosage was achieved in the desired time range of 5 minutes. While the paper described several over-simplifications and assumptions to achieve the results, the strategy is a good approach for practical industrial processes using plasma. Future work on plasma oxidation will likely involve MPC testing and implementation.

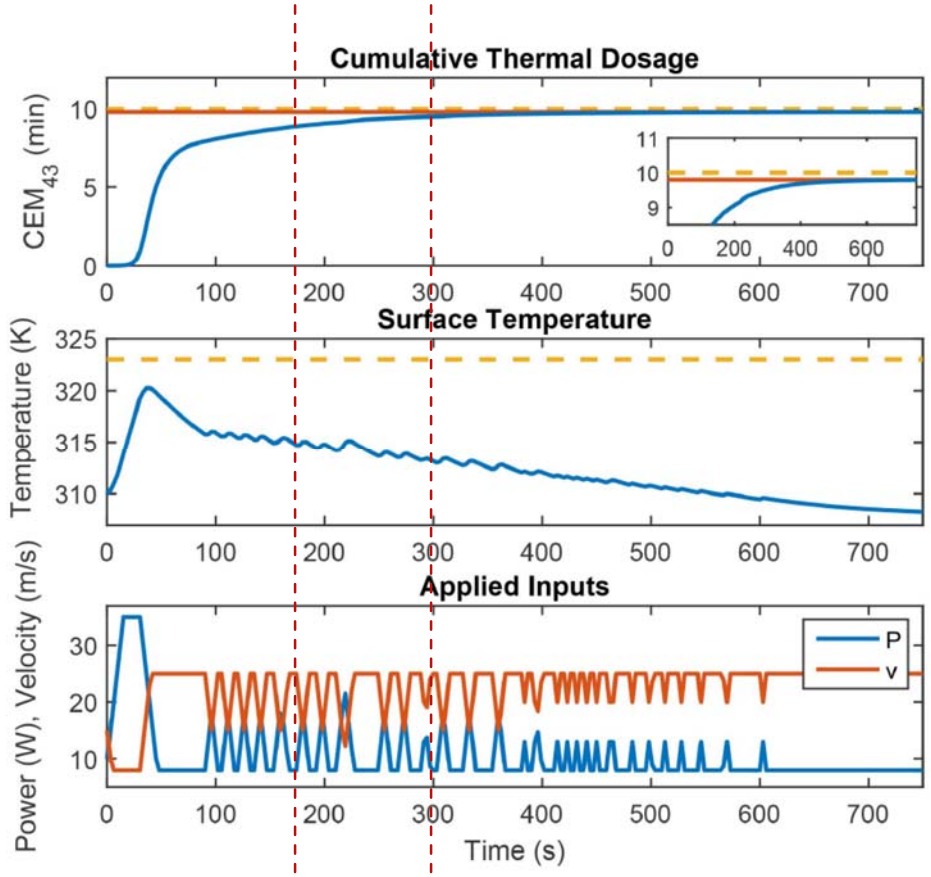

Figure 14: Results from the modeled MPC control strategy [16]**. The vertical dashed lines represent the target time range to deliver the dosage of CEM_{43}=10 min.**

Another example of a (albeit simple) control strategy is found in Patel et al [17]. In this work, the authors investigated replacing slats on an airplane wing with a plasma actuator with a closed-loop

control system. Two different feedback techniques were explored. Similar to the prior paper's claims, this paper claims to be the first publication looking at feedback control of a plasma actuator (2007). Construction of the plasma actuator is shown in Figure 15. The plasma is generated on the leading edge of the wing.

Figure 16 shows the plasma actuator installed on the airfoil in action in a wind tunnel. The left column is with the actuator off, and the right column is with it on. The top row is with the angle of attack of the airfoil at 16°, and the bottom row at 24°. Without plasma, both angle would result in a stall and loss of lift.

The control approach was more complicated in the area of processing more than anything else. There was one input, a high frequency pressure transducer, and output was simple on/off control of the plasma actuator. The control objective was to save power consumption by only energizing the plasma when it was needed. Therefore this doesn't qualify as an advanced control theory-based approach as in the previous 2016 article (leaving this author to believe in their claim of being the first to implement an advanced control method). The authors labeled this method the Amplitude Peak Sense and Control method. Another method was explored called the Pressure Amplitude Sense and Control method, but its process and ultimate outcome were similar to the first method and as such is not discussed here. Both looked at the frequency content of the pressure signal and took action based on that content. This approach is shown in Figure 17 below.

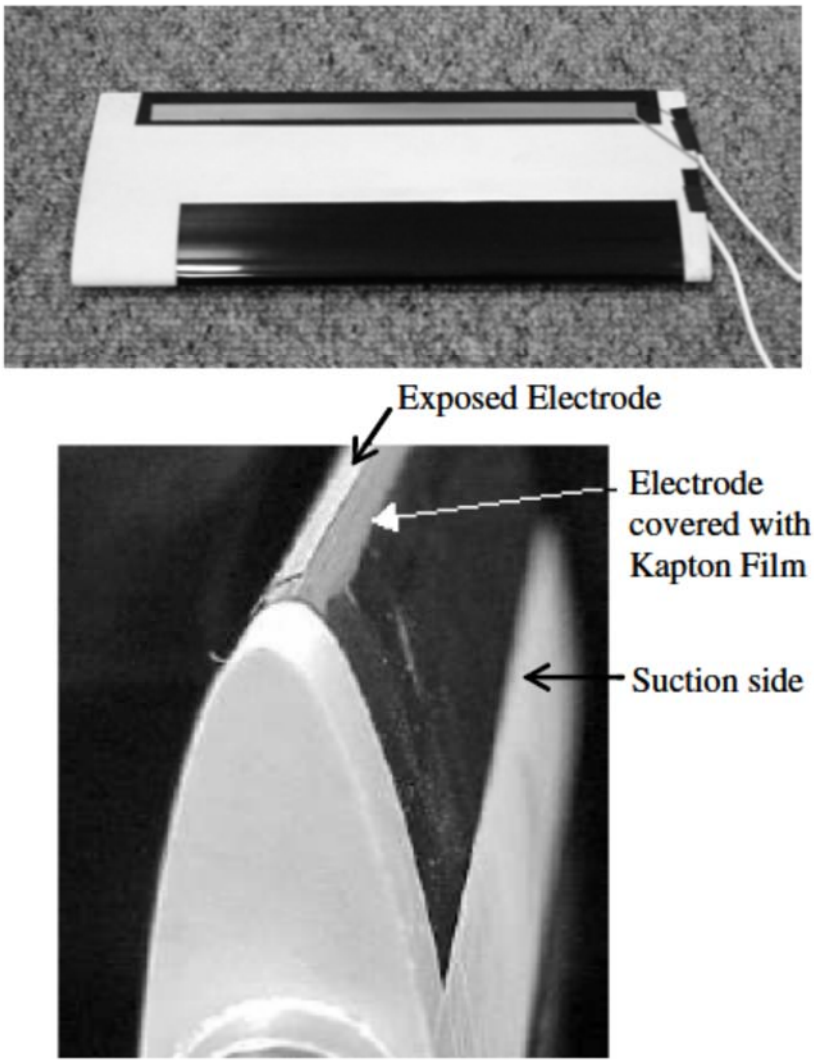

Figure 15: Design and construction of the leading edge plasma actuation [17].

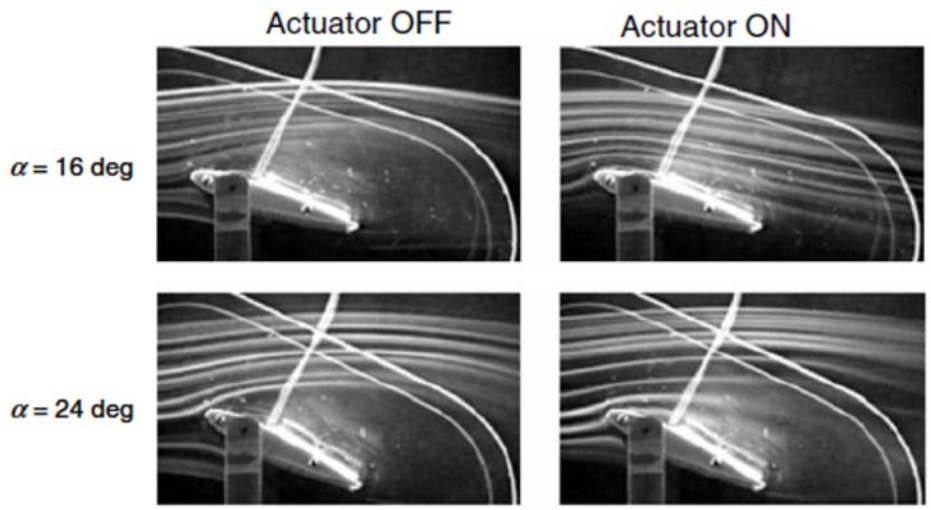

Figure 16: Plasma actuator demonstration in a wind tunnel [17].

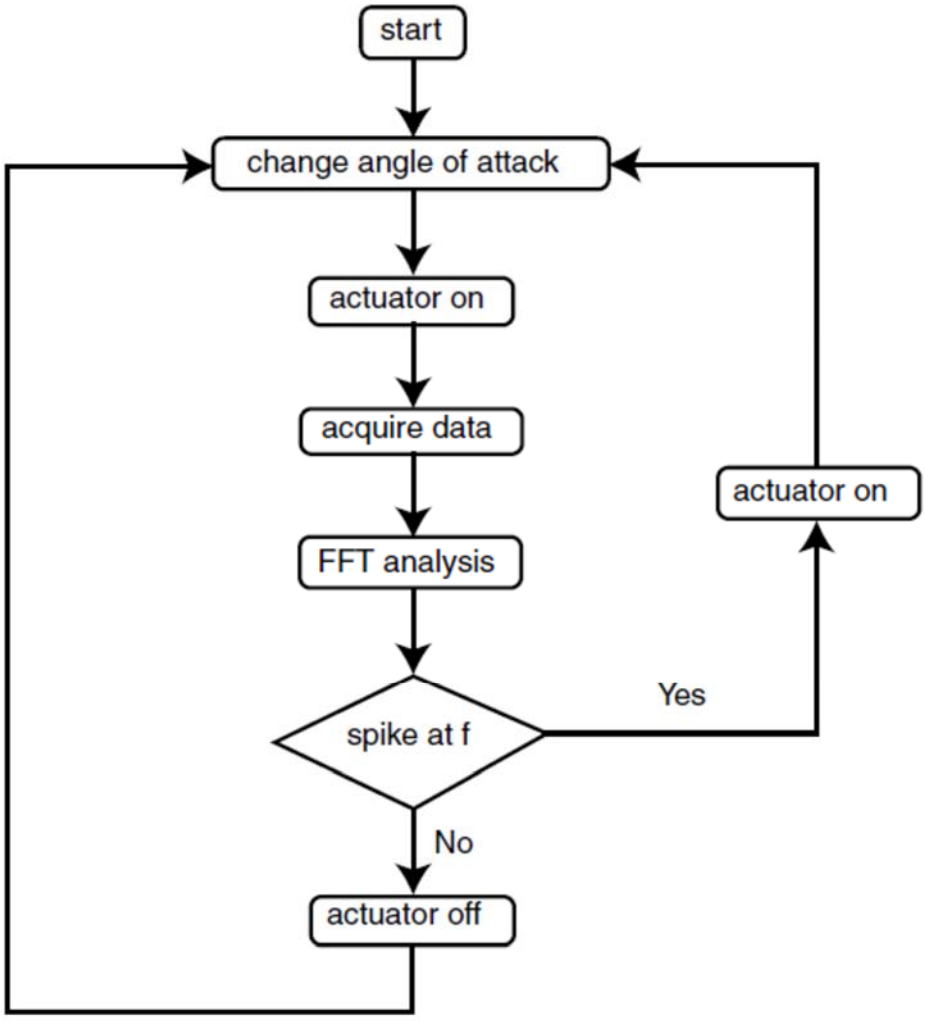

Figure 17: Control strategy for the plasma actuator [17].

The result of this approach was that the plasma actuator was successfully switched on when it was needed and switch off when it was not. There was no regulation of the plasma at all. An example of the power spectrum density information obtained from the static pressure transducer is shown in Figure 18.

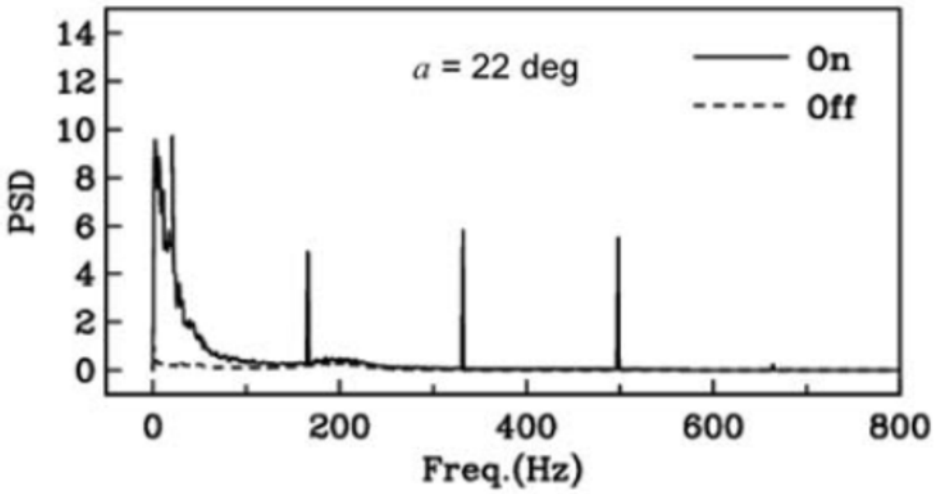

Figure 18: Power spectrum density versus frequency of the measured static pressure at an angle of attack of 22 degrees [17].

2.3 Precursor Oxidation

Conventional oxidation of carbon fiber precursor converts the polyacrylonitrile precursor from a thermoplastic to a thermoset, stabilizing the material both chemically and thermally so that it will survive the carbonization process. In a strict chemistry sense, the chemical stabilization occurs first, which is mainly thermally induced, and is followed by chemical oxidation reactions such as cyclization and dehydrogenation in the presence of oxygen [18]. Typically, a slow, well-controlled rate of heating is required to prevent run-away exotherms from damaging the fiber [19]. The process involves hot air and tension, with the fiber progressing through 4-8 independent zones of

processing, with temperatures progressively getting higher. The terms oxidation and stabilization are both used to describe this process, sometimes interchangeably, but in reality, both are occurring somewhat simultaneously. As is the case in industrial processes that experience rapid growth, the exact chemical reactions and mechanisms that the precursor undergoes during oxidation is still not well understood. It is generally accepted that there are three categories of reactions: cyclization (which includes cross-linking), dehydrogenation and oxidation [19]. The diffusion of molecular oxygen from the skin to core of each filament can be self-limiting, where the outer skin oxidizes and limits further processing of the core, resulting in a two-zone morphology in many cases. This is illustrated in Figure 19 below.

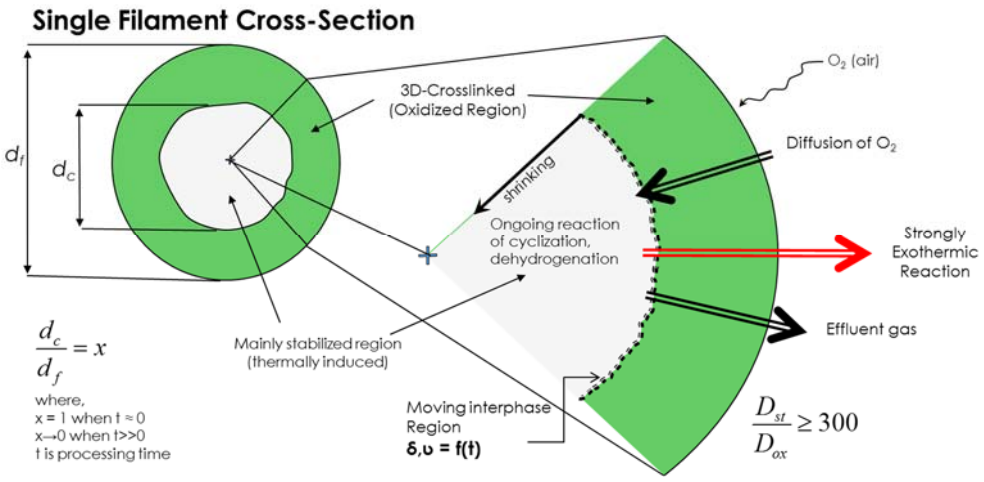

Figure 19: Illustration of the oxidation/stabilization process through diffusion into the filament [20].

where,

- d_f = the diameter of a single filament of precursor
- d_c = the diameter of the core defined by incomplete oxidation
- D_{st} = Oxygen diffusion coefficient through chemically stabilized PAN
- D_{ox} = Oxygen diffusion coefficient through fully oxidized PAN
- O_2 = molecular oxygen

- δ = radial thickness of oxidized region
- υ = radial thickness of the mainly stabilized region
- Effluent gas, gases that are released due to the chemical reactions taking place in the filament during oxidation

The diffusion of molecular oxygen through the filament is slowed as the filament is oxidized (i.e., $D_{st} > D_{ox}$). As the green zone grows, the rate of diffusion from skin to core drops. In addition, the level of crosslinking in the green zone constantly increases during oxidation further slowing down the rate of diffusion from skin to core. The rate can be increased with temperature, but if the temperature is increased too rapidly, run-away exotherms can result. A way around this limitation is to utilize oxidative species with smaller cross sections than molecular oxygen, such as atomic oxygen. While others in the field have tried various chemical means of accomplishing this, none are practical at the very large production scales that are used today [21]. Nevertheless, the concept is valid.

2.4 Prior Use of Plasma in Materials Processing

The application of plasma-based processing to carbon fiber manufacturing in general began with surface treatment [22]. Plasma surface treatment itself dates back to 1950s when corona discharge devices used to improve the wettability of plastic surface for printing, such as the treatment for the printing of plastic grocery bags [23]. It is natural and common to utilize industrial plasma technology for surface treatment of a variety of surfaces. What is uncommon is to utilize plasma for the bulk transformation of a material, which is exactly what plasma oxidation does. The exact method developed is described in the next section.

CHAPTER 3: PLASMA OXIDATION WORK ATRIBUTION

3.1 Plasma Oxidation Prior Work

The fundamental oxidation kinetics approach to accelerating the oxidation process was the original concept of Dr.-Eng. Felix Paulauskas of the Oak Ridge National Laboratory (ORNL). His original concept was to accelerate the oxidation process using oxidative species with lower molecular weights, i.e. lower mass, than molecular oxygen to improve the diffusion of these species towards the center of the precursor filaments. He explored various approaches to accomplish this using vacuum plasma and ozone generators at ORNL to expose the precursor to smaller molecular weight species (e.g., atomic oxygen via decomposition of ozone). It was demonstrated that oxidation did happen and fiber density did increase in shorter times than conventional. He then went to several different organizations to help with exploring various plasma technologies to progress the work, and eventually went to UT, where he met Danial Sherman who was a student at the time and also worked at a local technology company.

Discussions and preliminary work on plasma oxidation began in 2002, and the development of this technology began in earnest in 2004 as a joint effort between Dr.-Eng. Felix Paulauskas, and Mr. Daniel Sherman. The work was funded by the Department of Energy's Vehicle Technology Office as a means of achieving the office's stated cost reduction goals for carbon fiber as a means of vehicle lightweighting to meet future government mileage requirements. The two began small benchtop experiments to further explore feasibility. Several patents on this early work were filed [24][25][26]. This author became involved in the project in 2006. Mr. Sherman left the project in mid-2007, after which the collaboration continued between Dr.-Eng. Paulauskas and this author. The author transitioned this work to RMX Technologies in 2011, where it presently exists today. The collaboration continued through the combination of Dr.-Eng. Paulauskas' carbon fiber expertise and this author's plasma expertise, until its completion in 2015.

Early work between the first two researchers previously mentioned resulted in three published patents. The work was strictly experimental, as opposed to theoretical or computational. Successive reactor devices were built and tested, with each generation of equipment either testing theories or building on lessons learned from the prior one. These devices are shown in Figure 20 below. The first device shown (top left) was work completed at ORNL prior to any external involvement. This first device demonstrated some oxidation of the precursor, but had multiple problems, including no way to remove exothermic heat, welding of filaments, and damage of filaments. Therefore a progression of small benchtop devices were built and tested to enhance the advantages and remove the issues. The final device shown was termed the Single Tow Reactor 2 (STR2). The details of these devices are not presented in this dissertation.

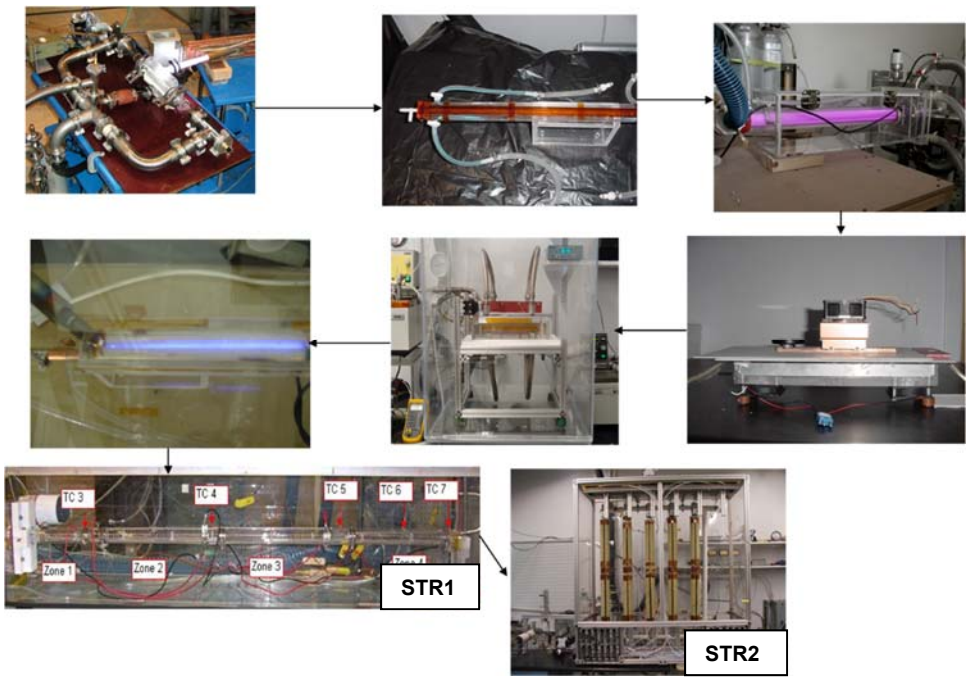

Figure 20: Hardware progression sequence before the author's involvement.

3.2 Contributions of the dissertation

The next four chapters cover the contributions from this author to the development of plasma oxidation. This section outlines the specific contributions made.

This author solely developed the plasma chemistry generation and delivery theory described in Section 4.1, based on his knowledge and expertise in the field of plasma engineering, and from experimental results obtained from activities under his leadership. In turn, the theory informed subsequent design changes and equipment modifications.

The author designed and picked out the control methods and associated hardware for the equipment discussed in this document, including writing the LabVIEW code presented in Section 5.2 (later versions were written by RMX staff).. He devised the control schemes presented in Section 5.3

The author designed all plasma generation electrode systems and selected all off-the-shelf components that were used in the power supplies for the equipment discussed in Chapter 6. He provided overall design guidance for all the experimental apparatuses. He led a team in the fabrication and assembly of all hardware discussed.

The author provided interpretation of results of both fiber properties and equipment performance to determine test matrices, future courses of action, and any required hardware/software modifications to improve the overall state of the technology.

CHAPTER 4: CLOSE PROXIMITY INDIRECT EXPOSURE THEORY

This chapter presents the theory of operation and physics behind the plasma oxidation of carbon fiber precursor. The first part will discuss the specific design and physics of utilizing atmospheric pressure nonthermal plasma to both generate and deliver highly oxidative chemistry to the fiber (or any other workpiece). The second part will present the mechanisms of how plasma chemistry impacts the oxidation of PAN precursor.

4.1 Plasma Oxidation Theory Part 1: Plasma Chemistry Generation and Workpiece Exposure

Traditionally, the hardware required for the plasma processing of materials is configured in one of two fashions. One is remote exposure (RE), in which the workpiece does not come into direct contact with the plasma but is usually placed at some distance or in a separate chamber from the plasma volume. Only the longest-lived chemical species generated by the plasma reactions survive to interact with the workpiece. While reactive species selection is limited by the separation between the plasma volume and the workpiece, additional control and chemical selectivity can be utilized by intermediate processing between the volume and the workpiece. The second arrangement is called direct exposure (DE), wherein the workpiece comes in direct contact with the plasma discharge volume. In this case the short lived species generated by the plasma can interact with the workpiece before they are lost to subsequent reactions. However, damage to a delicate workpiece such as acrylic fiber is much more likely with direct exposure. Through the discoveries and inventions made over the course of this work that are described later, a new technique called close proximity indirect exposure (CPIE) was developed and implemented. Here the physics and mechanisms of plasma oxidation of a workpiece using close proximity indirect exposure are described.

This part of the theory is focused solely on the optimization problem of generating and delivering the maximum amount of short-lived species to the workpiece. The optimization problem is solved by meeting the following objectives:

- Objective 1: Generate and deliver the optimum concentration of reactive species that accelerate the oxidation process to the workpiece.
- Objective 2: Accomplish Objective 1 in a spatially and temporally uniform fashion.
- Objective 3: Accomplish Objectives 1 and 2 in a way that is economically scalable to industrially relevant levels.

Objective 3 rules out many types of plasma generation systems, and even many conventional chemical generation systems. Neither thermal plasmas nor vacuum plasmas can be economically scaled to the very large levels required for industry adoption. This leaves nonthermal atmospheric pressure plasma sources as an option. Objective 2 rules out many of these latter sources that would be difficult to distribute uniformly over the many square meters of area needed. Objective 1 rules out any plasma generation system that depends on natural convective or unbalanced forced flow to deliver chemistry from the plasma to a workpiece not in direct contact with the plasma. The solution requires the efficient generation of plasma volumes that can span distances greater than ten meters and maintain uniform power density across such distances. It also requires a sufficiently close proximity between the plasma discharge and the workpiece such that short-lived chemical species generated in the plasma can survive long enough outside of the plasma volume to be delivered and react with a workpiece. A solution to this problem is the application of a surface dielectric barrier discharge with an asymmetric electrode arrangement that can accelerate neutral gas flow towards the workpiece using coupled electrohydrodynamic mechanisms.

4.1.1 Plasma Physics

The most common form of simulating plasma physics of a nonthermal plasma is with hydrodynamic modeling coupled to the relevant electrodynamics. The simplest version of this are

the continuity equations (8-11) coupled with Poisson's equation (11) referencing the electrically charged populations in the plasma volume [27].

$$\frac{\partial N_e}{\partial t} = S + N_e\alpha|\boldsymbol{W}_e| - N_e\eta|\boldsymbol{W}_e| - N_eN_p\beta_{ep} - \nabla\cdot(N_e\boldsymbol{W}_e - \boldsymbol{D}\nabla \mathrm{N}_e) \tag{8}$$

$$\frac{\partial N_p}{\partial t} = S + N_e\alpha|\boldsymbol{W}_e| - N_eN_p\beta_{ep} - N_nN_p\beta_{np} - \nabla\cdot\left(N_p\boldsymbol{W}_p\right) \tag{9}$$

$$\frac{\partial N_n}{\partial t} = N_e\eta|\boldsymbol{W}_e| - N_nN_p\beta_{np} - \nabla\cdot(N_n\boldsymbol{W}_n) \tag{10}$$

$$\nabla\cdot(\varepsilon_r\nabla V) + \frac{e}{\varepsilon_0}\left(N_p - N_n - N_e\right) = 0 \tag{11}$$

$$\boldsymbol{E} = -\nabla V \tag{12}$$

where,

- t is time
- N_e is the electron charge density
- N_p is the positive ion charge density
- N_n is the negative ion charge density
- $\boldsymbol{W}_e$ is the electron drift velocity*
- $\boldsymbol{W}_p$ is the positive ion drift velocity*
- $\boldsymbol{W}_n$ is the negative ion drift velocity*
- $\boldsymbol{D}$ is the electron diffusion coefficient*
- α is the ionization coefficient*
- η is the attachment coefficient*
- β_{ep} is the electron-positive-ion recombination coefficient*
- β_{np} is the negative-ion-positive-ion recombination coefficient*
- S is the photo-ionization source term
- ε_r is the relative permittivity (dielectric constant)*
- ε_0 is the permittivity of free space
- V is the electric potential
- e is the electron charge
- $\boldsymbol{E}$ is the electric field

*These transport properties are based on the type of gas being used, and can be pulled from various sources in the literature.

In words, equations (8-10) state that the partial derivative (rate of change) with respect to time for the electron charge density, the positive ion charge density, and the negative ion charge density,

respectively, are equal to the sum of various sources and sinks of those populations. Specifically for equation (8), the time rate of change of electron charge density is equal to the sum of the photoionization of oxygen (which, in a two-step process can lead to new electrons [28]) with ionization reactions, minus attachment reactions, electron-positive ion recombination reactions, and the divergence of (or outward flux caused by) the difference between the electron charge drift and the spatial spreading, or diffusion of electrons).

4.1.2 Electric Field

In the plasma oxidation optimization problem, the first goal is to maximize the ionization rate of the plasma volume. The ionization rate is represented as the partial rate of change with respect to time of the positive and negative ions (the populations of both can increase simultaneously). From the continuity equations, both the electron and positive ion charge densities are increased by the ionization (α) initiated by the electron population as well as the photo-ionization effect. The negative ion charge density is increased by the attachment reaction (η) of electrons with oxygen (which is the second-most electronegative element in the periodic table – thus an oxygen-containing plasma can generate negative ions). Therefore, α, η and S are all terms that should be maximized in the plasma generation design. Both $\propto$ and η are exponential functions of electric field and pressure, where increasing the electric field raises their values, and the increasing pressure lowers their values. In the paper previously cited [27], the photoionization source term S was based on a physical model that, in summary, is based on the ultraviolet emission from nitrogen molecules that is absorbed by oxygen molecules resulting in photoionization of those molecules. The greater the oxygen content in air, the greater the photoionization effect. In the plasma oxidation scenario, the pressure is fixed around atmospheric pressure and cannot be modified, and the oxygen content essentially remains the same as standard atmospheric conditions. This leaves the electric field as the dominate handle on increasing the rate of ionization – at least in this simplified model. Boundary conditions, such as surface charge

accumulation, secondary-electron emission (the release of electrons from a solid surface caused by electron bombardment), and photoemission (the release of electrons from a solid surface caused by light) must also be considered in any analysis of a surface discharge. Nevertheless, all of these functions are directly proportional to the electric field. Therefore, in this instance, the maximization of the electric field is essential for maximizing the total ionization rate.

4.1.3 Frequency

Excitation frequency is another important parameter, and its effect on the above equations is seen in the applied voltage, which creates a dependency on time. In the case of a pure sinusoidal function:

$$V(t) = |V| \cos(2\pi f t + \varphi) \tag{13}$$

Where,

- $|V|$ is the magnitude of the voltage
- t is time
- f is frequency
- φ is phase

Nevertheless, a plasma engineer normally is not entirely free to choose any frequency desired. There are many constraints in its range. The choice of frequency impacts hardware complexity, cost, compliance issues, and safety considerations. In the case of a dielectric barrier discharge, the operating frequency is mostly a function of the excitation method constrained by the electrode design and size as well as impedance matching method. In the case of the present work, it was deemed most practical to operate in the VLF (very low frequency) range. Therefore, again, applied voltage becomes the main input to the system.

This conclusion does not imply that the solution is to simply maximize the applied voltage from the power supply system. What is critical is that the plasma electrode geometry and materials are designed in such a way as to maximize the electric field created from a given power delivered by the power supply. By definition, the electric field is the spatial gradient of the applied voltage

between the electrodes. The spatial rate of change of the potential is a critical factor in the electrode design and excitation signal utilized. However, equation (13) is not the strict definition used in Poisson's equation, since its dependence on space is not represented, and the gradient (∇) and divergence ($\nabla \cdot$) are spatial operators. The voltage at any point in space between the cathode and anode is dependent on the electrode design, including geometry and materials used, so a spatially dependent voltage function, $V(x, y, z, t)$ would be design-dependent. This allows a plasma engineer to determine exactly where the plasma will exist and where it will not. By utilizing proper electrode design and materials selection, the maximum electric field strength can be produced for a given power delivery.

One may ask about how electric current plays a role in the plasma design and discharge. The continuity equations show the time-dependent behavior of the charges involved, which, by definition, is the electric current, since 1 Amp is 1 Coulomb per second. This means that the electric field again is the main handle on electric current in this situation. The other control the plasma engineer has on current is in the electrode design itself. Electrode material, size, separation distance and arrangement have a strong influence, as well as dielectric barrier material properties and thickness. So electrode design is a critical element to the process. In summary, electric field optimization through electrode design and operational optimization is critical to the successful implementation of optimal plasma chemistry generation.

4.1.4 Electrohydrodynamics

With plasma chemistry generation optimized, the next step in the process is delivering this chemistry to the workpiece as efficiently and quickly as possible. Fortunately, with proper electrode design, a unique set of physics can be brought to bear that takes advantage of charged particle behavior in an electric field with momentum laws of fluid dynamics. This phenomenology is referred to in the literature as electrohydrodynamics [29][30][31][32][33]. Like the fluid dynamics

modeling approach of plasma physics, the force produced by this phenomenology can be characterized in a variety of ways. One of the more simple expressions is [33]:

$$\boldsymbol{F}_{EHD}(t) = \sum_i q_i \int n_i(\boldsymbol{r}, t)\boldsymbol{E}(\boldsymbol{r}, t)dV \quad (14)$$

where,

- q_i is ±*e* (electron charge)
- $n_i(\boldsymbol{r}, t)$ is spatial and temporal distribution of the charged particle species
- $\boldsymbol{E}(\boldsymbol{r}, t)$ is the spatial and temporal distribution of the electric field

The index, i, refers to the three charged populations, electrons, positive ions, and negative ions. What is most interesting in equation (12) is the lack of representation of mass. An intuitive examination of the electrohydrodynamic (EHD) force would naturally lead to the conclusion that electrons play a minimal role due to their minimal mass. There is some debate in the literature as to whether this is true [33] or not [34]. From the latter reference, charged particle momentum equations are used to define the EHD force, and include charged particle mobility, μ. This mobility is inversely dependent on mass:

$$\mu = \frac{q}{m\nu_m} = \frac{q}{kT}D \quad (15)$$

Therefore from this interpretation, the total EHD force should be minimally impacted directly by electron motion, aside from the fact that it is the electrons that truly transfer energy from the electric field to the ions themselves.

Figure 21 illustrates how, through proper electrode design, an EHD force can be taken advantage of to rapidly deliver short-lived reactive species generated by the plasma to the workpiece without direct exposure. In this illustration, the brown and gray structures are one embodiment of the plasma electrodes (other designs and arrangements are possible). The blue ovals represent the plasma discharge. The yellow and green arrows demonstrate the continuous circulation of flow to and from the plasma discharge and the workpiece (black line), specifically in this case fiber.

The green arrows represent gas flow with fresh reactive species coming from the plasma, while the yellow arrows represent background air getting sucked into the plasma. Appropriate material selection, electrode geometry and arrangement, and distance from the plasma to the workpiece are essential design steps that impact the overall effectiveness of the process. Figure 21 is a generic embodiment of the plasma oxidation process.

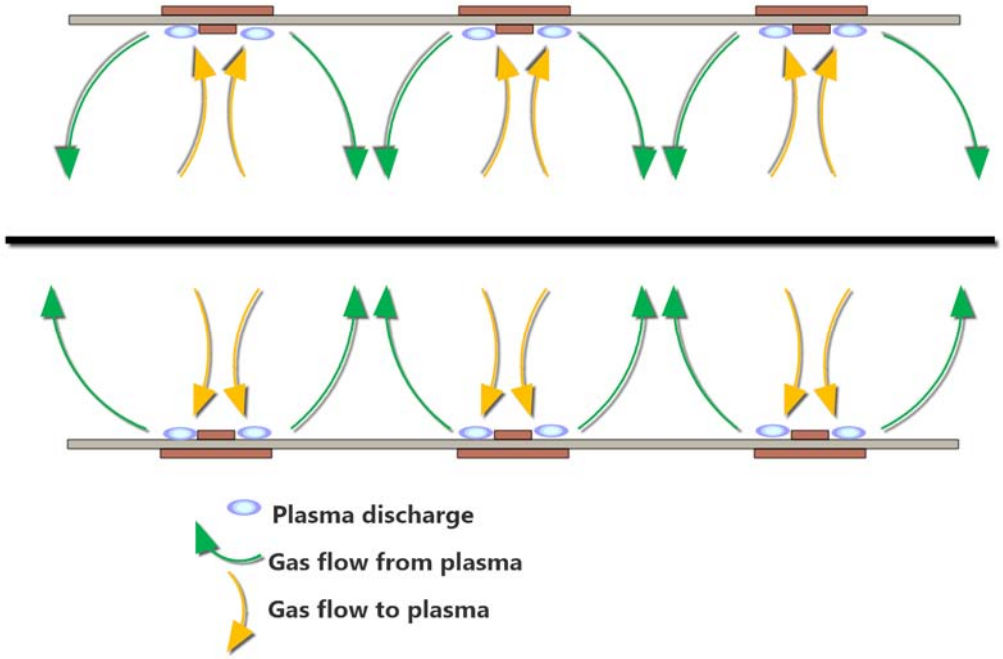

Figure 21: Illustration of the electrohydrodynamic force.

4.1.5 Aerodynamics

Proper air flow and the uniform manipulation of that airflow across the width of the process volume is critical for proper processing of the fiber. Air is injected into a contained treatment volume where the workpiece exists. The workpiece can be inserted in a batch-like process, or on a continual basis. The method of air injection can vary, and can range from continual fresh air injection to recirculation of air with partial fresh air injection. The air is typically heated before

injection to a certain minimum temperature in order to achieve sufficient reaction rates within the bulk of the workpiece. A certain percentage of air passes through the plasma volume, where it interacts with the discharge physics. This interaction produces the plasma chemistry that is accelerated to the workpiece through the EHD effect. The aerodynamic design of the treatment volume must ensure that forced airflow does not disrupt the EHD delivery mechanism.

4.1.6 Thermodynamics

The plasma also provides supplemental heating to the treatment volume through dielectric heating of the dielectric barrier of the electrode structure itself. This heating mechanism can be quantified as [35]:

$$P = kE^2 f \varepsilon'' \tag{16}$$

where,

- k is a unit dependent constant
- E is the electric field
- f is the frequency
- ε'' is the loss factor

This heating mechanism, coupled with the proper materials, is much more efficient at thermal production per watt of electrical input than a resistive heating element. However, care must be taken to balance the power deposition into dielectric heating versus plasma generation and chemistry production. As one can see from equation 16, the thermal power from dielectric heating is proportional to the frequency, as well as the electric field squared. This makes the heating mechanism highly sensitive to the electric field derived from both the electrode design and the excitation signal.

4.1.7 Plasma Chemistry

The importance of proximity is critical, as many of the most reactive species generated by a plasma in air are extremely short lived due to dissociation and recombination reactions that take

place after their creation. While the author did not have access to the necessary equipment to take direct in situ measurements during processing, an excellent reference is provided by previous simulation work by Eliasson and Kogelschatz examining the reactive species generated by a nonthermal plasma in simulated air (20% O_2, 80% N_2). A chart of resulting lifetimes is shown in Figure 22.

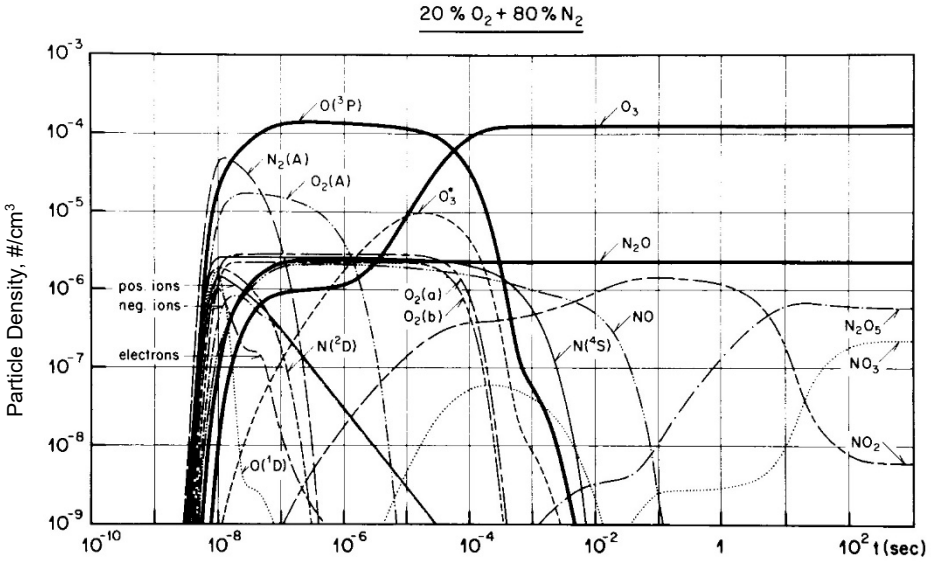

Figure 22: Chemical reactions initiated by an air plasma [36].

This graph shows the lifetimes of various oxygen and nitrogen based reactive species once they have left the plasma volume (in this particular case, after a single short pulse of plasma). The vertical axis is the particle density (number of particles per cubic centimeter) and the horizontal axis is time after plasma pulse ignition. The reactive species shown here are various states of atomic nitrogen and oxygen ($O(^1D)$, $O(^3P)$, $N(^4S)$ and $N(^2D)$, where the number and letter in parenthesis represent the electronic state of the atom [37]), ions and electrons, metastables ($N_2(A)$, $O_2(A)$, $O_2(a)$, and $O_2(b)$), and other oxidative molecules (O_3, NO, N_2O, N_2O_5, NO_3, NO_2). One free radical is shown here, $O^{\cdot}_3$, and in actual air, where hydrogen is usually present in the

form of water, ˙OH is generated as well. It is important to note that under certain conditions, metastable lifetimes can be much longer than shown here [1].

Figure 23 shows an estimated overlay of the three exposure methods discussed at the beginning of this section: direction exposure (yellow), close proximity indirect exposure (green), and remote exposure (red). The EHD effect can accelerate flows to 10 m/sec or higher. At a 1 cm distance, this puts lifetimes in the range of 10^{-4} to 10^{-3} seconds into play. For the conditions discuss in the reference used here [36], atomic oxygen can be made to react with the workpiece. This conclusion is further reinforced with additional analysis performed by [38]. This work focused on pulsed corona discharges. The evaluation of oxygen species lifetimes is shown in Figure 24.

In addition, the effect of humidity can play a significant role in producing additional oxidative species, such as OH, HONO or $HONO_2$ that can play a role in the oxidation reactions in the workpiece [39]. In the typical oxidation oven, humidity will always be present in some degree, so its effect must be taken into account.

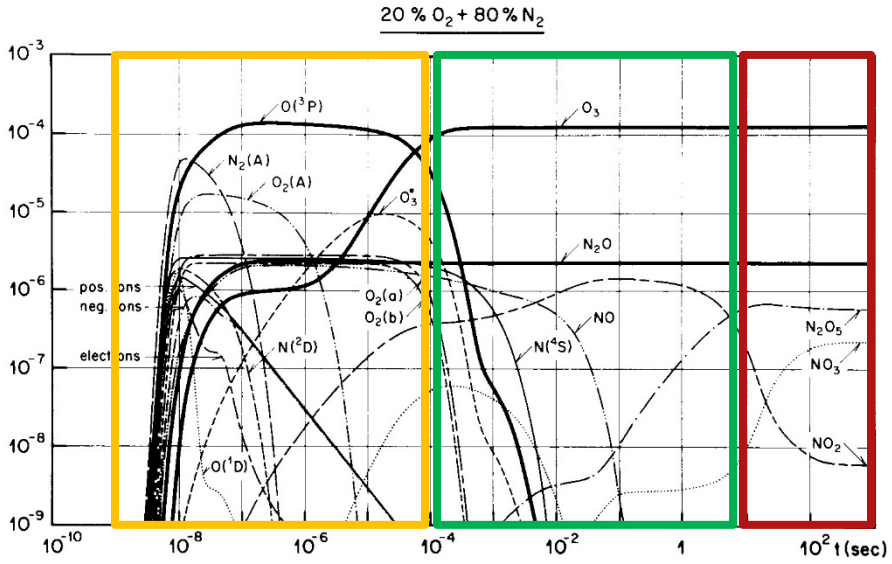

Figure 23: Same plot as shown in Figure 22, but delineated by the three plasma exposure methods.

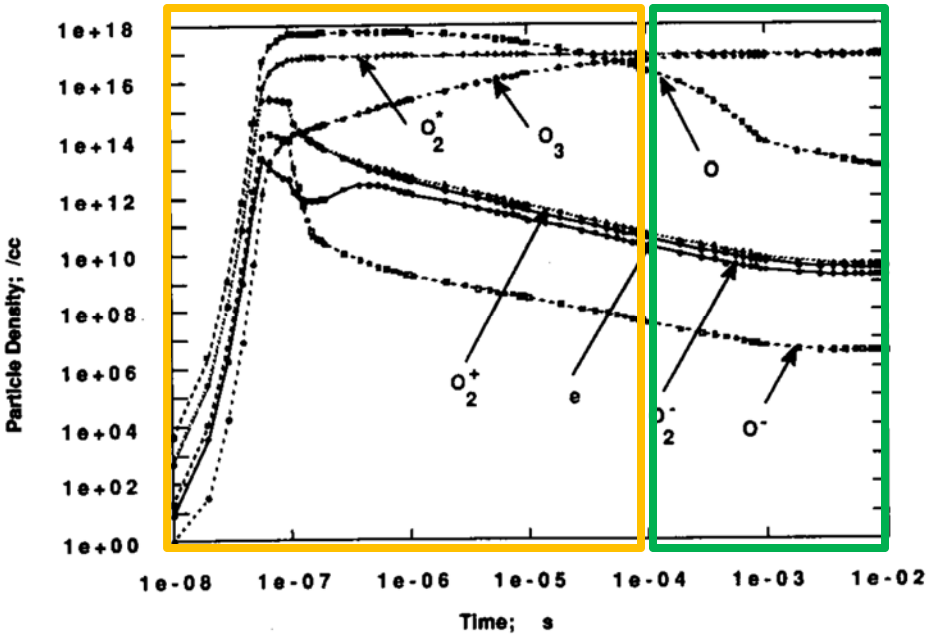

Figure 24: Oxygen species lifetimes [38].

4.1.8 Contaminated Plasma

With plasma chemistry mechanisms being of prime concern in the plasma oxidation process, issues surrounding contamination, from both gaseous and particulate sources, must be addressed in the theory. The plasma oxidation workpiece is typically polyacrylonitrile fiber that is undergoing chemical transformation. Part of this transformation includes the release of byproducts such as hydrogen cyanide, ammonia, carbon monoxide, carbon dioxide, water and tars [5][19]. All could be considered gaseous contaminants except for the tars, which could be considered particulate contaminants. Water and carbon dioxide have the greatest concentration, but even so the overall concentration is very low during oxidation. Both of these contaminants actually can contribute to the plasma oxidation process by providing oxygen species for the plasma to break down. The two non oxygen-containing species, hydrogen cyanide and ammonia exist at such low concentrations in the oxidation stage [19] that their effect on the plasma chemistry would be minimal. Tars coming from the fiber represent floating particulates in the process gas stream. At full scale production levels, these tars exist at fairly low concentrations. Nevertheless particulates can have a major impact on plasma physics, so much so that an entire field exists in this area called dusty or complex plasma [40][41]. At sufficient concentration, particulates, whether they are vapor droplets or solid particles, collide with electrons and ions, accumulating charge. With sufficient charge, these particulates become an added species in the plasma population (particulates, ions, electrons and neutrals) and can strongly influence the overall space charge distribution. This effect is lessened at high pressure levels such as atmospheric pressure, but can still exist. A study on the impact of particulates in plasma actuators [40] found that particulates can influence the overall velocity produced by the EHD force, although this difference was not significant. Figure 25 shows the measurement made in this study.

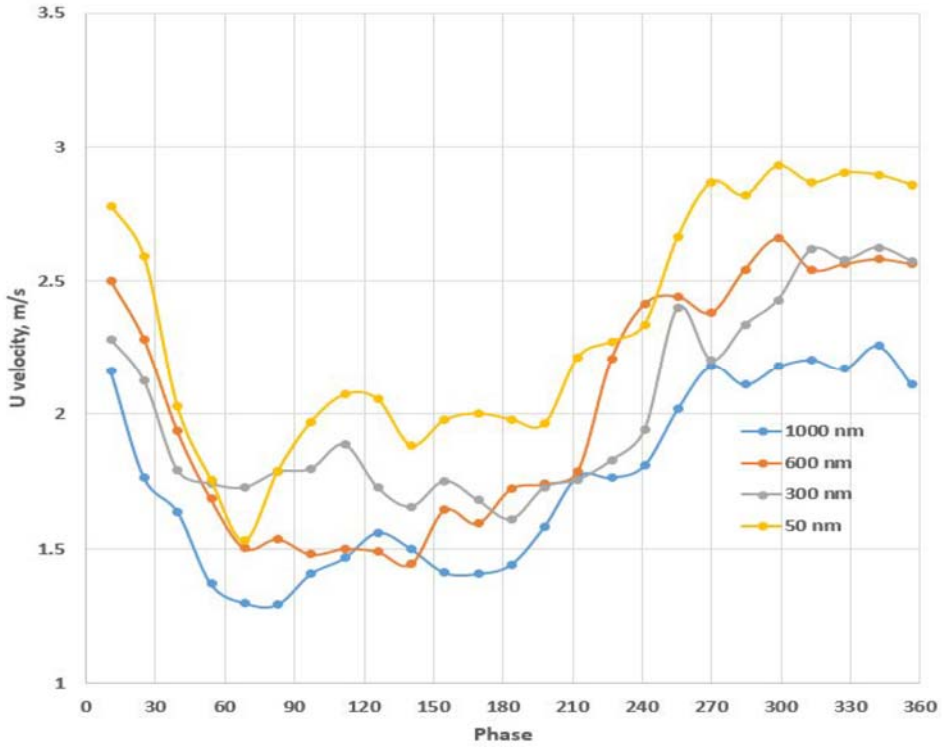

Figure 25: Net velocity for different particulate sizes in the plasma versus excitation signal phase [40].

4.2 Plasma Oxidation Theory Part 2: Fiber Transformation

A way to implement a chemical acceleration mechanism at production scale is with nonthermal plasma. When implemented properly, plasma can provide a large-scale economical means to generate highly oxidative reactive species that can accelerate the stabilization process of carbon fiber precursors. An illustration of the difference between the conventional oxidation and plasma oxidation processes is shown in Figure 26. In that figure, the three progressions from top to bottom have split cross-sections to illustrate the chronological difference in chemical change due to the reactive species generated by the plasma (shown in orange). This illustration is used to show the acceleration possible due to the plasma. The actual transformation of the filament is much more complicated than shown.

In the progression from top to bottom of the illustration, it is seen that the diffusion from the skin to the core of the filament of plasma-generated reactive species progress much faster than the diffusion of molecular oxygen. As previously discussed in section 2.2, the rate of diffusion of molecular oxygen through the filament can only be increased by increasing the filament temperature. In contrast, the reactive species generated by the plasma have much higher diffusion rates on average.

The reactive species created by the plasma volume are more reactive than molecular oxygen, and have smaller collisional cross sections that allow them to diffuse faster through the bulk of the filament. The impact that the collisional cross section size has on particle interactions is illustrated in Figure 27 below. The larger the collision cross section, σ, the greater the probability that the particle in question will collide and possibly react with particles in its path. The reactions shown are elastic collisions, where the total kinetic energy is conserved between the two particles, and their states do not change. In contrast, for plasma oxidation reactions to be beneficial, inelastic collisions, such as those listed in Table 1 (except for the elastic scattering reactions) are desired.

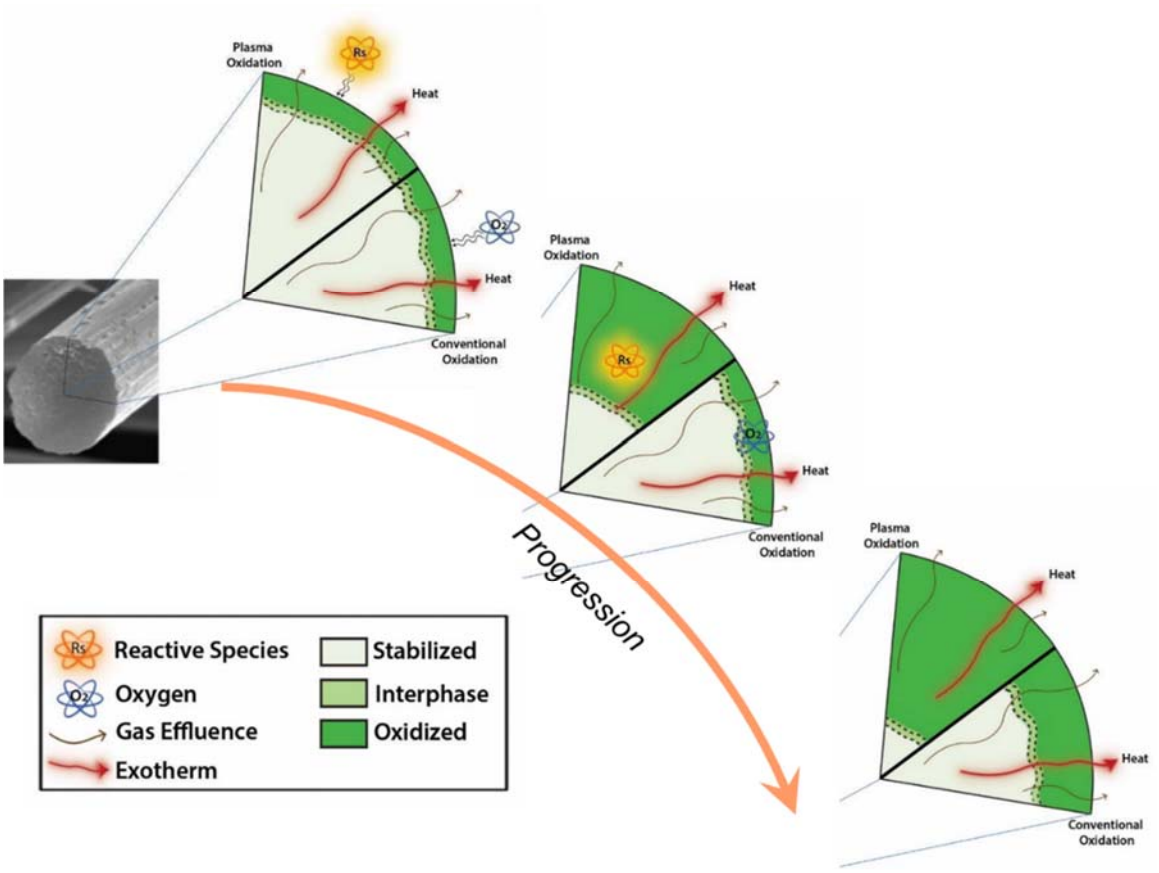

Figure 26: A simplified comparison of two oxidation mechanisms.

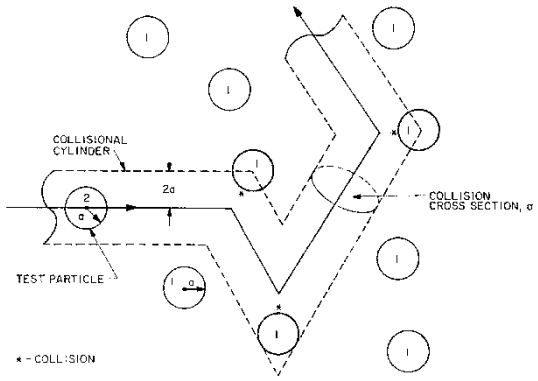

Figure 27: Illustration of the effect that collisional cross sections of a particle how on its interactions with other particles [3].

The relationship between the collisional cross section of a particle and its mean free path is defined as [31]:

$$\sigma = \frac{1}{n\lambda} \tag{17}$$

where,

- σ is the collisional cross-section
- n is the particle number density
- λ is the mean free path

The net result of this faster diffusion mechanism is the reduction of the required oxidation time anywhere from 2.5X to 5X from the conventional process. The actual reduction depends on the specific precursor chemistry and processing conditions that were executed. Specific results are presented in Chapter 7.

CHAPTER 5: CONTROL THEORY AND METHODOLOGY

5.1 Scope and Hardware

A unified control scheme is essential to properly controlling the plasma chemistry's effect on the fiber. Several variables play a role in successful processing. LabVIEW hardware and software was utilized for control and automation of the process of both the MTR1 and the SMR2 as well as the recording of data for subsequent analysis. The schematic shown in Figure 28 illustrates the connection arrangement for the SMR2. In it, one can see that a data acquisition system (DAQ) was designed to communicate with every device that controlled the influential process parameters, the majority of which were:

- Temperature: As with any chemical process, temperature plays a strong role in the reaction kinetics. For the oxidation process, a minimum temperature is necessary to initiate the chemical transformation, while a maximum temperature is defined by a state of exothermic runaway, where the rate of heat released from the fiber is so great that it damages the material.
- Fiber control: The fiber itself must be precisely drawn through the oxidation oven with both line speed and stretch controlled. The stretching of the fiber ensures proper molecular alignment of the polymeric chains.
- Gas flow: Air is dried and delivered with defined flow rates and pressures. Uniform distribution of gas flow within the oven ensure uniform processing of the fiber along the width of the tow or tows.
- Plasma: Several plasma parameters are controlled, while others – critical to performance – are not. Those that are not relate to the geometrical arrangement and materials used to construct the plasma electrodes, and the power electronics designed to maximize power transfer from the power supply to the plasma volume. The controlled parameters include voltage, duty cycle, and frequency, all of which contribute to the overall power density of the plasma volume.

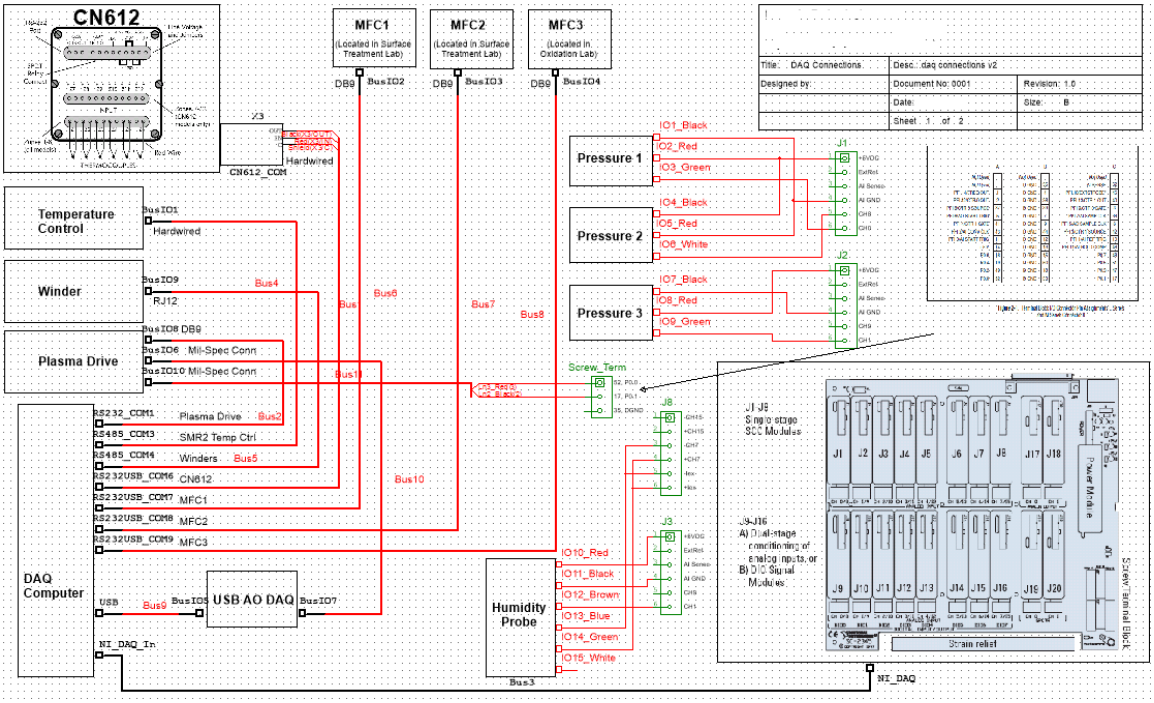

Figure 28: Schematic of general interface among major components of the SMR2.

5.2 Control Software

In addition to hardware design, control code written in National Instruments LabVIEW development environment and was utilized to control and record all measured data in the SMR2. Examples of both the control interface, and the underlying source code (which is graphical in its implementation, similar to Matlab's Simulink) are shown in Figure 29 and Figure 30.

Figure 29: LabVIEW control interface for SMR2.

In the above figure, the panel for plasma control is displayed. The section labeled *Scope Readings* displays values of voltage, current, frequency, and power taken directly from high voltage probes wired to the plasma discharge electrodes. The section directly adjacent to the right labeled *Power Supply Readings* displays similar information, but from the power supply. Contrasting the two sets of readings permits the evaluation of the efficient transfer of power which can be optimized through impedance matching, described in the next section.

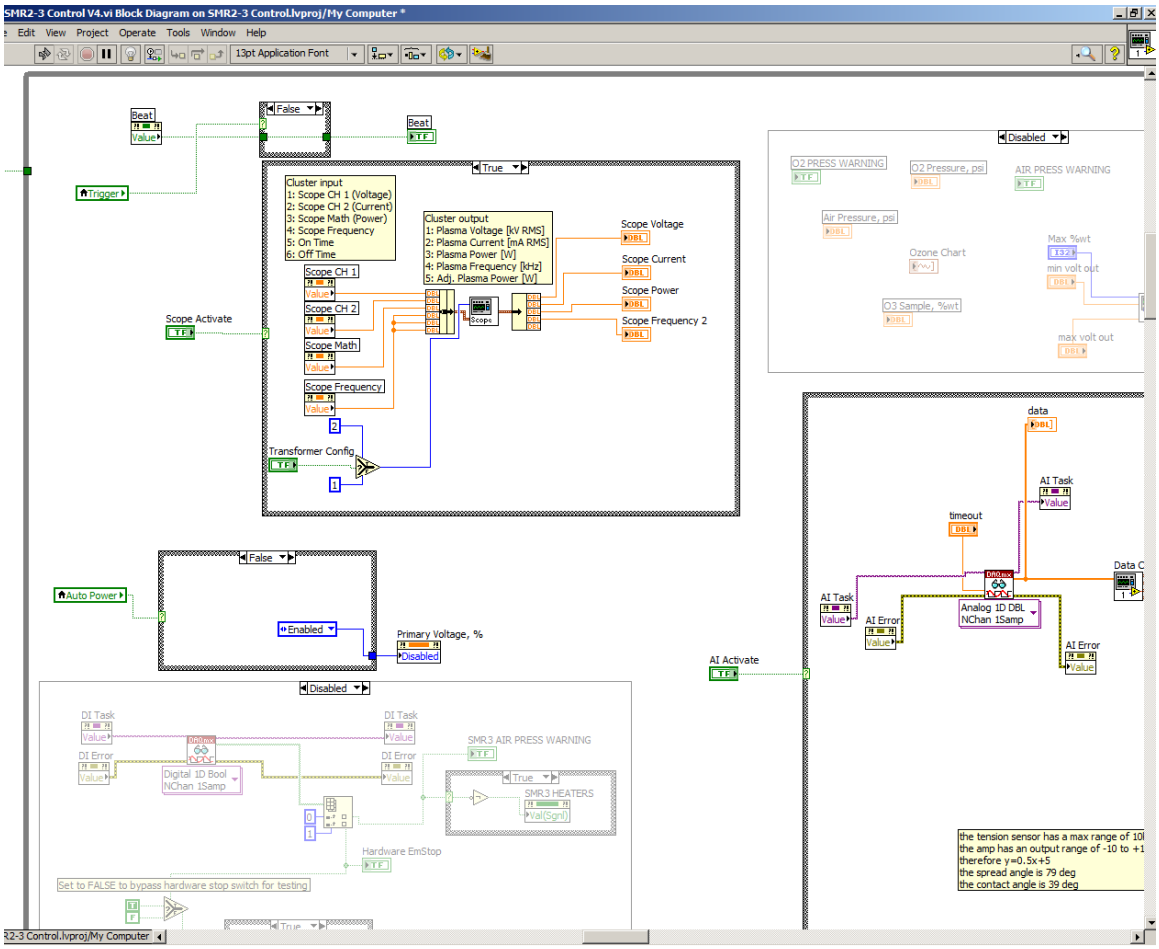

Figure 30: LabVIEW block diagram of plasma control section.

The *Power Supply Control* section contains the controls for the plasma power supply. One can see the PID controller here, which is discussed in the next section.

5.3 Control Methods

5.3.1 Feedback for Plasma Control

In the early operational stage of the 1 aMT plasma oxidation oven, the plasma was controlled in an "open-loop" fashion by setting the plasma power independently of other oven conditions. Control of plasma power and temperature are coupled variables due to the fact that the plasma introduces thermal energy into the oven beyond that provided by the conventional heat sources. Control of temperature is simplified when the plasma power is simply held constant. This was one mode of operation implemented in the 1 aMT oven, but other control algorithms were explored. An example of one such control scheme is the combination of holding certain heat sources constant and make the plasma power controlled by a desired temperature set point in the oven. In this case, the plasma can change the temperature of the oven much more rapidly than the conventional heat sources can, lead to a more finely controllable temperature adjustment. The PID algorithm was utilized here, and is discussed in the next section. This control approach is illustrated in Figure 31. Other control schemes were tested but cannot be discussed in this work.

5.3.2 Control Algorithms

In several instances, proportional-integral-derivative (PID) feedback controllers were utilized. These devices have the following transfer function in the *s*-domain [42]:

$$G_c(s) = K_1 + \frac{K_2}{s} + K_3 s \tag{18}$$

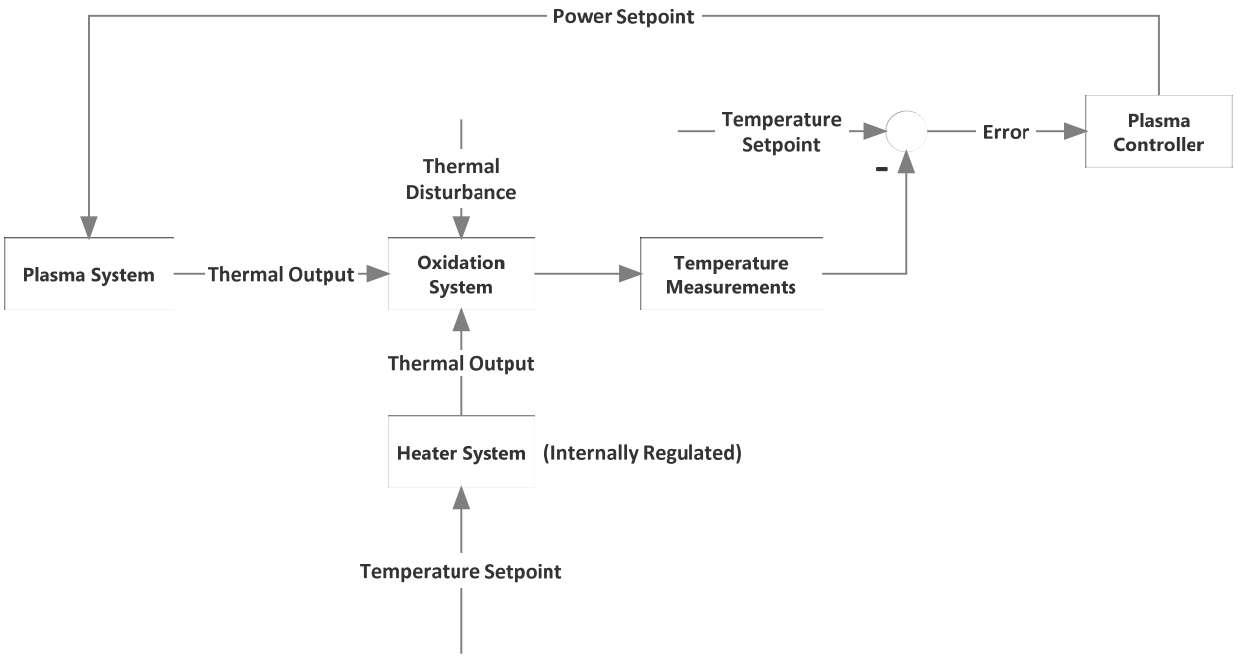

Figure 31: One example of a plasma power control scheme that was explored.

where,

- K_1 is the proportional gain
- K_2 is the integral gain
- K_3 is the derivative gain

By properly tuning the three gains, robust control is achieved for the given parameter under a variety of environmental conditions. Tuning was accomplished by either automated means or manual techniques, such as the Ziegler-Nichols method [43]. This latter method is only an option if the system being tuned can tolerate significant oscillation of the control parameter, which wasn't always the case in this work. This type of control was utilized for temperature, tension, line speed, and experimental auto plasma power modes of operation.

Several methods of automatic plasma control based on parameters in the equipment, such as temperature or fiber properties were explored. In the future, model-based automation could be implemented as a robust control solution.

5.4 Impedance Matching

In addition to design and fabrication of the embedded plasma electrode system, significant work was required to determine the best way to energize the system. Unique impedance matching arrangements were tested and optimized. Inverting power supply cores were purchased off-the-shelf and modified to deliver optimal power and integrate with the entire system. Impedance matching of the power supply to the plasma generating electrodes was a critical step in producing sufficiently high plasma power density. This, along with the electrode construction itself, allows for instantaneous plasma power generation sufficient to produce the desired reactive species. An ideal impedance match will completely cancel the reactance of the load so that the power supply sees a purely resistive load across its terminals. Zmp is the primary side matching components (in the figure represented by simple inductors but could be more complicated), Zms is the secondary side matching components (with same comment about complexity), and the

plasma generation circuit represented by a capacitive, partially rectified resistive load. Figure 32 shows an equivalent electrical circuit representation of the excitation signal arrangement for the plasma generation system.

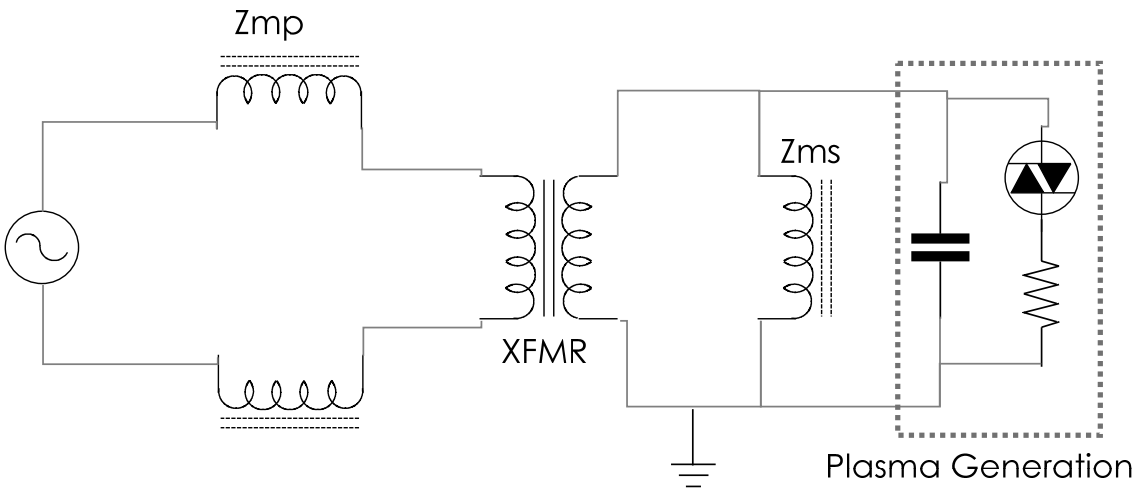

Figure 32: Approximate equivalent circuit of plasma generation for oxidation.

While such a situation is practically impossible, good matches can be obtained where 60% or more of the real power can be transferred to the plasma discharge itself in the form of ionization and dielectric heating.

For a given impedance matching arrangement, examples of the voltage, current and power mapping of the plasma power system are shown in Figure 33 through Figure 35. The “% Voltage” parameter on the y-axis is simply the gain control from 0 to 100% of the available full power. The “frequency” on the x-axis is the main excitation frequency of the power signal. The z-axis alternates between measurements made across the plasma electrodes. The “voltage”, “current”, and “power” parameters are the measured root-mean-squared (RMS) values of the plasma

discharge itself. The colors represent binned values of the z-axis, and are identified in the legend on the right.

The efficiency of reactive species production versus input power is dependent not only on proper impedance matching, but on electrode construction. Since such details remain proprietary, it can only be said that instantaneous power density of the plasma volume, a critical parameter of reactive species production efficiency, is a function of geometry and materials selection of the electrode design. The scalability of plasma generation over large areas is also directly impacted by electrode design criteria.

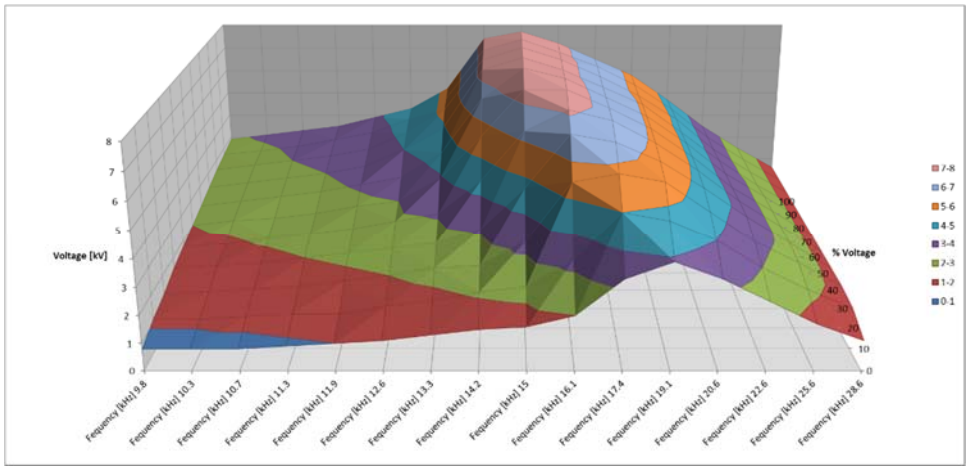

Figure 33: Plasma voltage map versus frequency and gain (% voltage).

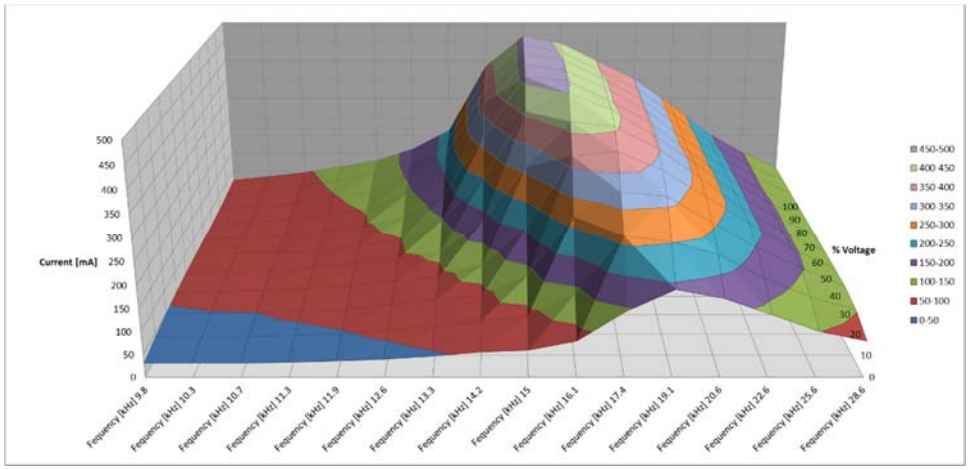

Figure 34: Plasma current map versus frequency and gain (% voltage).

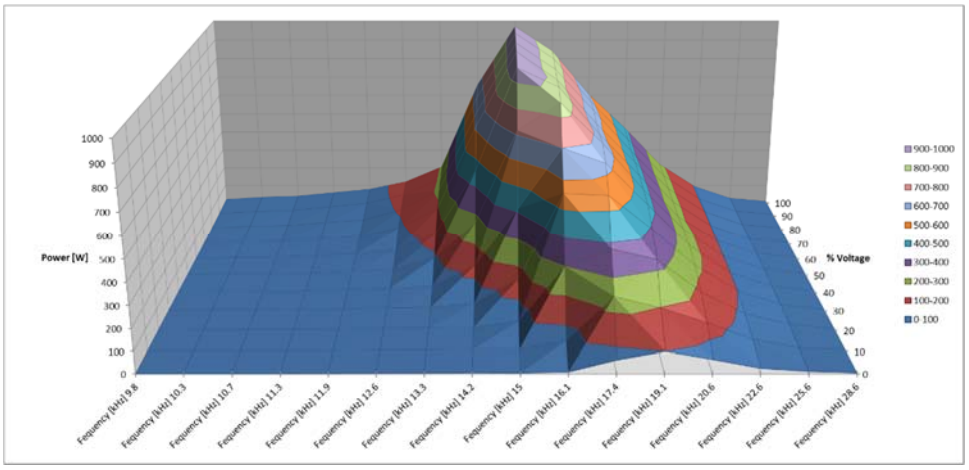

Figure 35: Plasma output power map versus frequency and gain (% voltage).

CHAPTER 6: HARDWARE DEVELOPMENT

This chapter outlines the progression of experimental apparatus that were designed, built and operated to test the different plasma processing methods and scale up the technology to the 1 aMT (annual metric tons of fiber nameplate) capacity.

6.1 Single Tow Reactor 2

The purpose of the STR2 was to continue testing of the remote exposure (RE) method explored with the previous reactor, the STR1, but with longer processing length to produce oxidized precursor faster than the previous device. Each of the six vertical glass tubes shown below were fed with a gas stream coming from a separate plasma generator (similar to the one shown in the middle image of Figure 41) and had independent temperature control via heating wire coiled around each tube. Therefore this device could slowly heat the fiber in six steps enabling more precise control and reliable performance of the oxidation process. Flow and composition of the gas feeding the plasma was controlled by multiple mass flow controllers. The plasma generator gas flow path was 12-16 feet from the plasma volume to the reactor. Results from this device were very good and led to a new patent application on which this author is an inventor [44]. This device was operated until 2009, when the Multiple Tow Reactor 1 (MTR1) became operational.

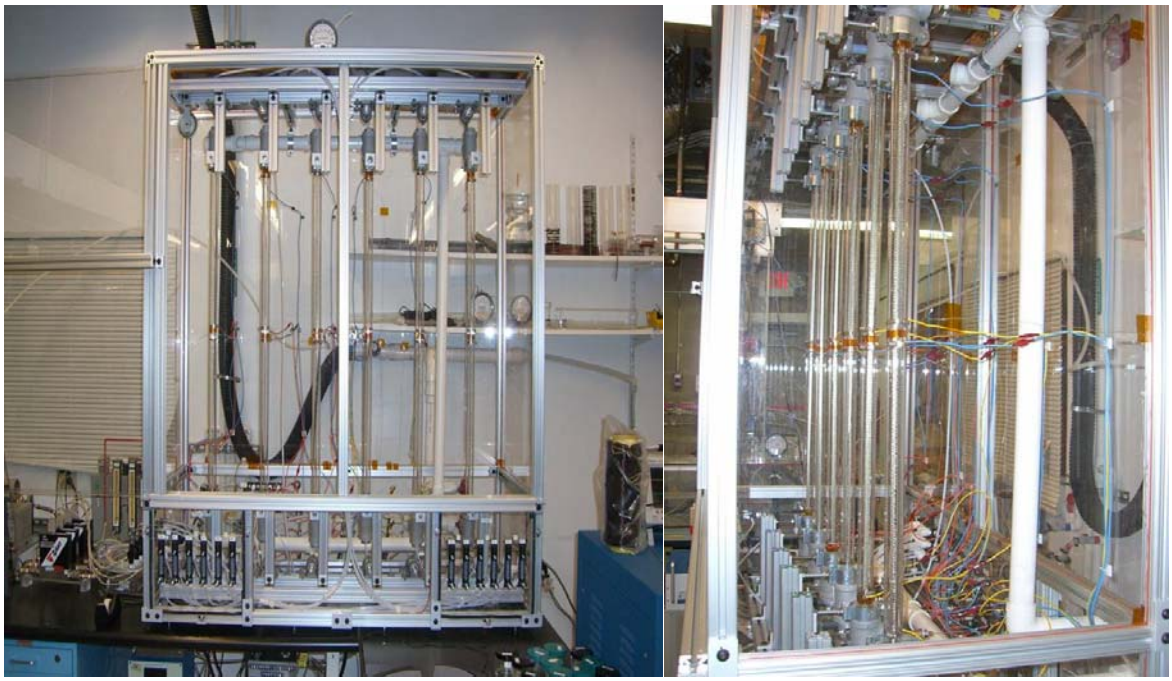

Figure 36: Plasma Oxidation Single Tow Reactor 2 (STR2) using remote exposure.

6.2 Multiple Tow Reactor 1

Due to the success of the STR2, a scaled-up version was planned that incorporated all of the functional advantages of the STR2, but with the additional capability of processing multiple fiber tows simultaneously. This became the Multiple Tow Reactor 1, or MTR1, which was designed and built in a new facility in 2009. A CAD drawing is shown in Figure 37, and the final apparatus shown in Figure 38 and Figure 39. It utilized the same RE principles as the STR2, but with a single, rectangular cross section to permit up to six tows of precursor inline. It had size thermal processing zones and multiple injection points for plasma gas insertion. This was the first plasma oxidation reactor to utilize National Instruments LabVIEW software and associated hardware to implement an automated control and logging scheme. Initial results were interesting but problems with the performance of the device led to various issues including fiber damage. Expectations were never met with respect to fiber performance as will be seen in the next chapter. The challenges were related to the scalability of the RE processing approach that had been the main focus of the project to date.

After several different configurations and modifications were made to the MTR1 with minimal improvement, focus shifted to coming up with a different, scalable way of exposing the fiber to the plasma discharge. This investigation led to a completely new exposure technique discussed in the next section, which turned out to be much more effective and scalable than any method or apparatus previously examined.

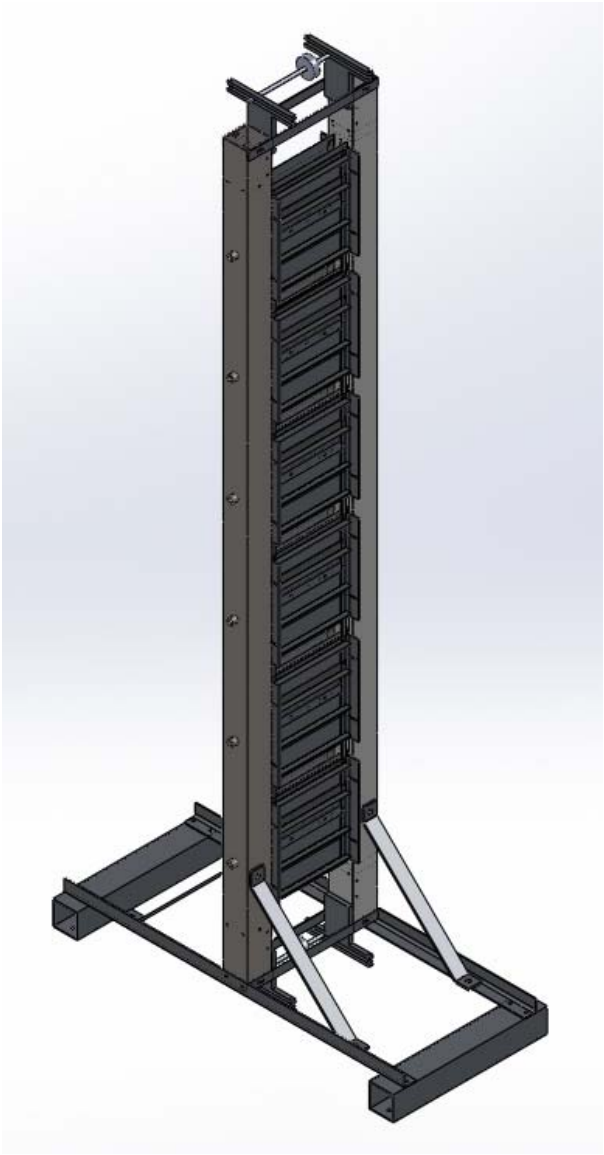

Figure 37: Computer aided drawing of the Multiple Tow Reactor 1.

Figure 38: Plasma Oxidation Multiple Tow Reactor 1 (MTR1) using remote exposure.

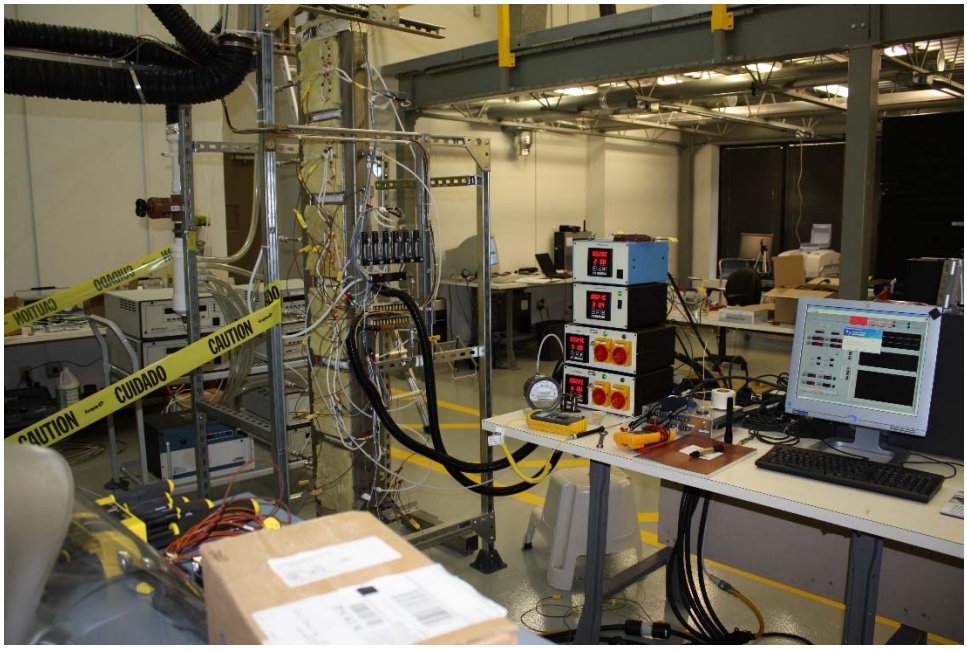

Figure 39: Plasma Oxidation MTR1 side view with LabVIEW control computer.

6.3 Close Proximity Indirect Exposure Development

Due to the shortcomings of the MTR1, work began in 2010 on an alternative method maximizing the advantages of plasma processing while minimizing the problematics issues associated with the RE method as implemented in the MTR1. The author's specific invention and major contribution, which occurred in 2010-11, was a new exposure method that combined the best advantages of the two previous techniques, remote exposure and direct exposure, and was termed *close proximity indirect exposure* (CPIE). The theory of this method has already been discussed in Chapter 4. Direct exposure of carbon fiber precursor was tried in the early years and ruled out as it resulted in damage to the individual filament surfaces (see middle-left image of Figure 20). Remote exposure was explored from when this author began in 2006 through 2011 that gave early good results, but eventually was limited in throughput as the process and equipment was scaled up. A simplified illustration of the difference in implementation of the three methods is shown in Figure 40. In all three versions, the hashed rectangle represents the workpiece being acted upon by the plasma.

The differences in actual hardware between the three exposure methods utilized in this work are shown in Figure 41. In the left image, the fiber is directly immersed in the vertical plasma volume. In the middle image, only the plasma volume is shown. The fiber is in a separate chamber not shown, with the gas coming out of the plasma being pumped to the fiber. In the right image, the fiber is being drawn through a treatment chamber where plasma is being generated.

Special materials were required for the construction of the plasma electrodes to produce the proper plasma while surviving the harsh conditions of the chamber. Figure 42 is taken from the issued patent document concerning this invention and illustrates several key functions. The stars represent plasma generation on the lower surface of the chamber. The plasma itself accelerates the surrounding gas and generates vortices as illustrated that serve to circulate thermal energy and the reactive species generated by the plasma.

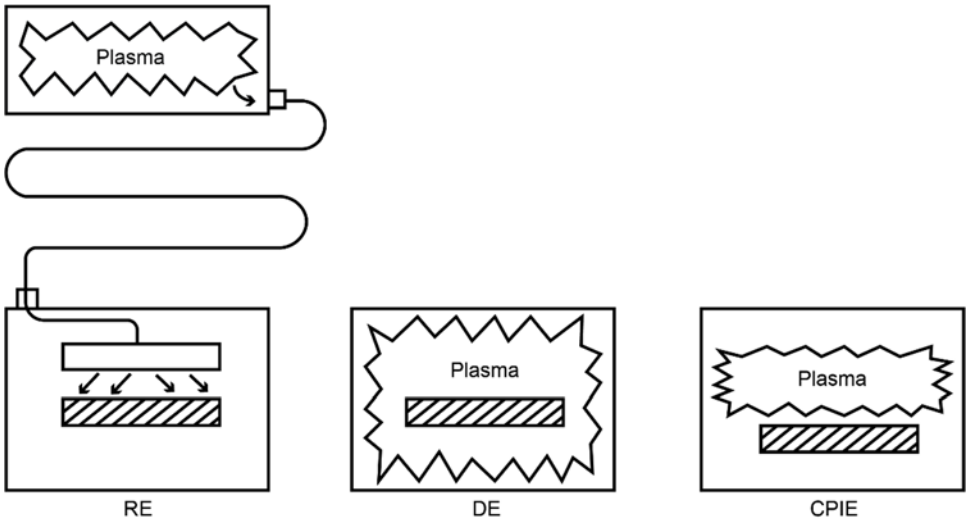

Figure 40: Illustration of different methods of exposing a workpiece to the effects of a plasma volume; plasma remote exposure (RE), direct exposure (DE), and close proximity indirect exposure (CPIE).

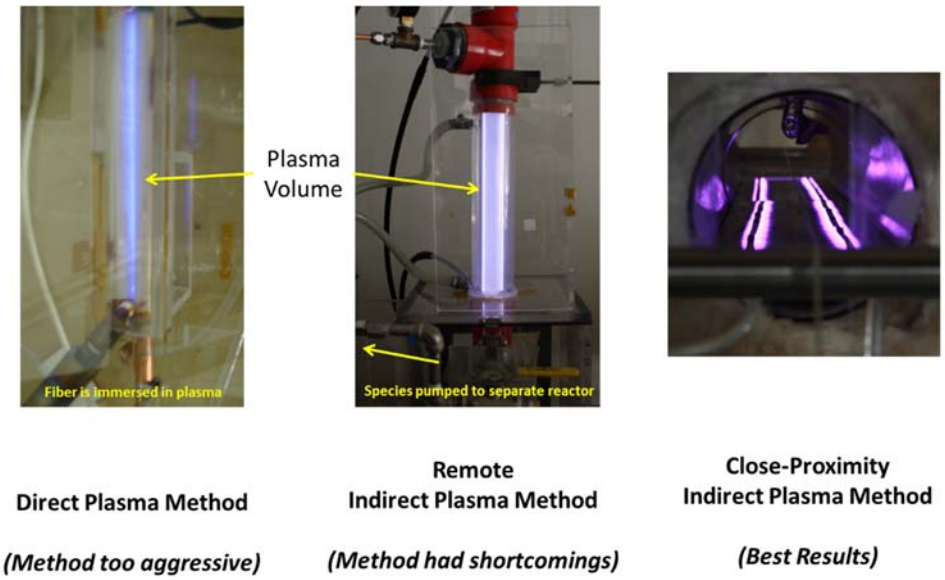

Figure 41: Illustration of the plasma generation devices involved in the three different exposure techniques utilized in this work.

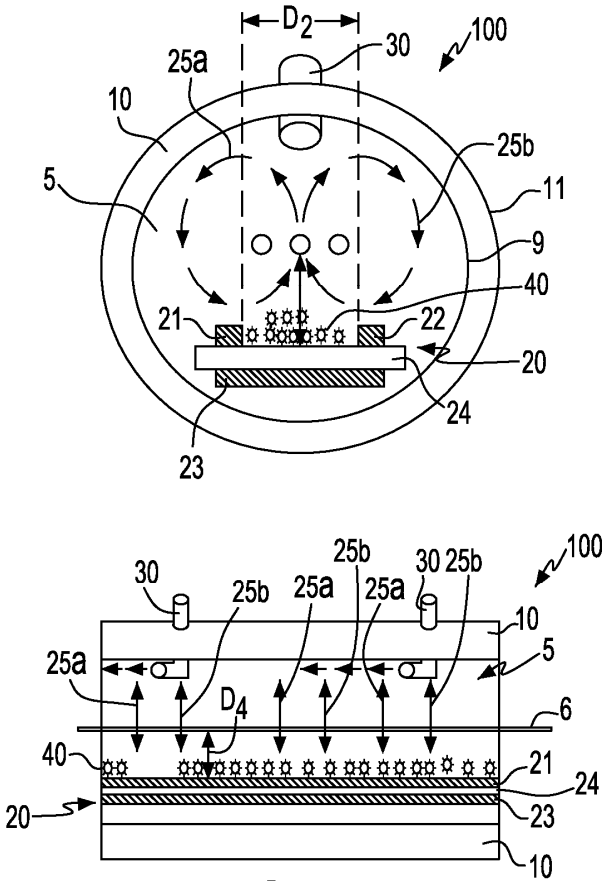

Figure 42: Top and Side illustrations of the new close proximity indirect exposure plasma oxidation system [45].

Due to the proper selection of materials, the plasma generates significant thermal energy very efficiently, lessening the need for external conventional heat sources. Oxidation of the fiber is an exothermic process, so at a certain point in the process the flow vortices begin to act in a cooling function to draw heat away from the fiber and prevent damage to the filaments. The CPIE technique was developed in a separate test stand, but once the design was firmed up, testing on fiber was ready to commence.

6.4 Surface Modification Reactor 2

A device that had been built for another project involving a separate technology called plasma surface treatment was available to test the CPIE oxidation technique. This device was termed the Surface Modification Reactor 2 (SMR2) and is shown in Figure 43. It required significant modification for testing the new plasma oxidation technique.

This oxidation technique, already mentioned previously as CPIE, takes advantage of two phenomena: 1) The introduction of the plasma volume directly into the treatment volume, yet not in direct contact with the fiber. It is positioned in “close-proximity” to the fiber in such a way as to bring in to play short-lived reactive species generated by the plasma volume, as described in detail in Chapter 4. 2) A general electrode configuration that can accelerate background gas flow. A unique configuration was devised that generates aerodynamic flow vortices that provide uniform heating and cooling of the fiber while accelerating the short-lived reactive species to the fiber, reducing the time of flight required, and thereby raising the concentration of these species at the surface of the fiber.

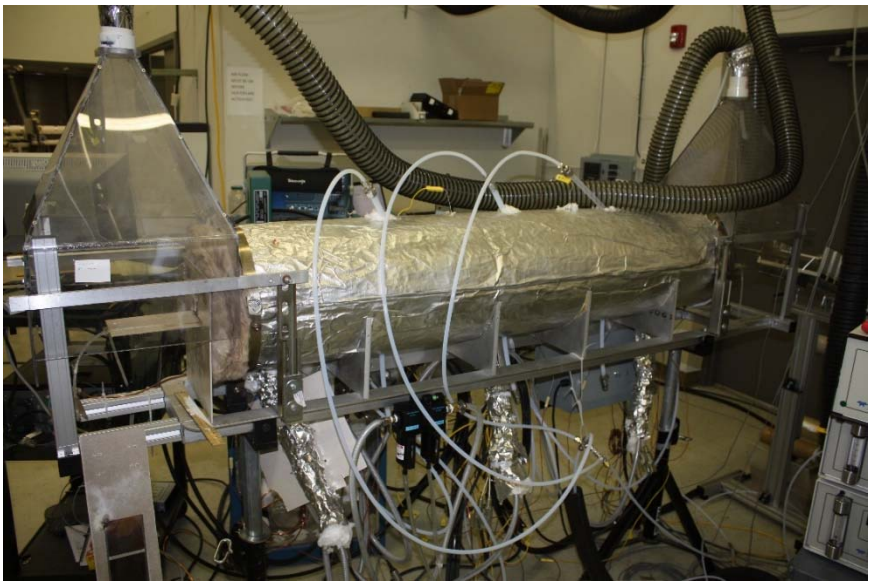

Figure 43: Surface Modification Reactor 2 (SMR2) converted for use with plasma oxidation close proximity indirect exposure.

Due to the fact that the SMR2 was not originally designed for plasma oxidation, some sacrifices were made with respect to functionality and performance. This device only had three thermal processing zones that were not thermally isolated from each other. This made thermal control of the entire process a challenge. In addition, fiber stretching could not be independently controlled through each zone, impairing the overall fiber property results. Nevertheless, even with these constraints, fiber properties and oxidation rates were dramatically improved over any previous experimental results achieved to date, as will be seen in the next chapter. This device was operated from 2011 through 2013, and demonstrated the accelerated affect that plasma can bring to bear on the fiber by decreasing the required residence time from 80 minutes to 20-30 minutes for small tow carbon fiber precursor.

6.5 1 aMT Multiple Tow Reactor 2

With the success of the SMR2 in achieving significantly decreased processing time while maintaining fiber properties, it was decided to scale up this new CPIE approach to the 1 annual metric ton (aMT) level. The design approach of this oven was to mimic, as much as possible, the layout and configuration of production scale conventional ovens, as shown in Figure 44 (without any fiber handling equipment). Certain aspects of conventional processing remained unchanged with plasma processing, such as the need for multiple independent processing zones where temperature and tension could be precisely set for each stage of oxidation. This oven was designed with an 8 inch effective processing width, 4 independent processing zone of plasma power, fiber tension, temperature, and air flow. As with the previous equipment, this oven was completely designed internally and all associated equipment was either off-the-shelf or custom fabricated by contract machinists or internally. The power supplies utilized off-the-shelf generators that were integrated into a larger power generation system that was optimally impedance matched to the custom plasma electrodes installed inside the oven. Four power systems were configured for each processing zone so that independent control was possible. An

important detail that may not be obvious in Figure 44 is the fact that the top two “modules” have a different design than the bottom two modules, or zones. Due to the fact that the modules needed to be stacked on top of each other because of space constraints in the laboratory, the bottom modules had three pass-through slots for the fiber to pass through those modules in three continuous runs, coming out on the opposite side of the entrance. The fiber then was routed vertically upwards into the module directly above the first, where it made only two passes through it before coming out on the same side as the entrance and proceeding straight through to the third module. The second and third processing modules (the top two modules) had to be longer than the bottom two in order to achieve the same processing residence time.

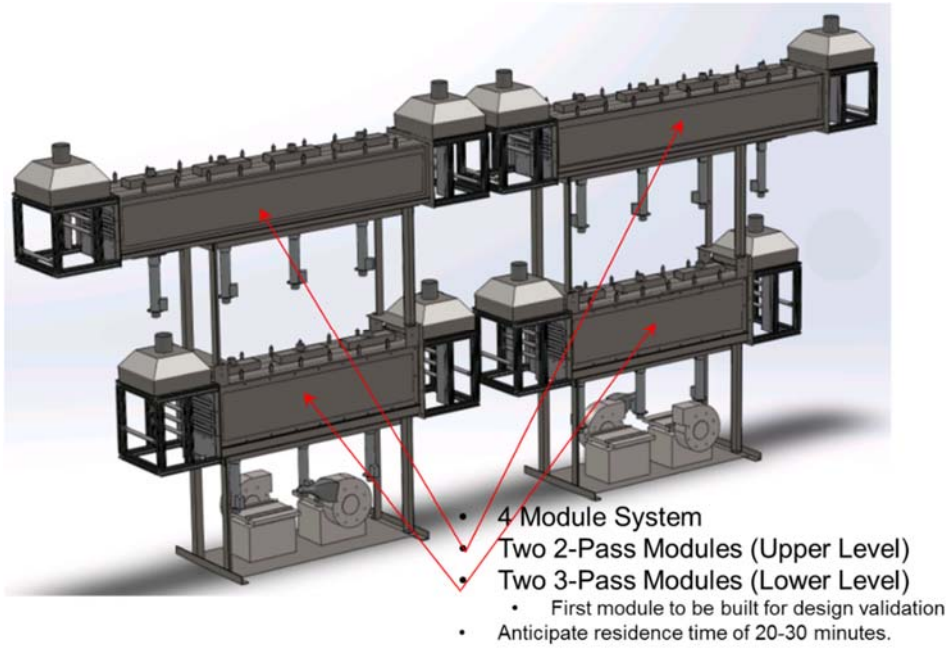

Figure 44: Design illustration of the Multiple Tow Reactor 2, the 1 annual ton plasma oxidation oven.

Due to the design differences in the top and bottom modules, the plasma electrodes installed in each were respectively different and had to be designed for each specific module. This required

other subtle differences in the impedance matching approach and other electrical engineering details.

Figure 45 shows an image of the MTR2 soon after installation being setup for initial trial runs in 2014. The fiber handling equipment was designed to handle up to six medium size tows of 48,000 filaments or less, or one large size tow up to 300,000 filaments. Multiple fiber types and oven configurations were tested over the two years from 2014 to the present, with hundreds of hours of operation seen by the oven. An image taken in 2016 is shown in Figure 46. The specifications and capabilities of the Multiple Tow Reactor 2 are shown in Table 4.

Figure 45: Image of the Multiple Tow Reactor 2 during initial setup.

Table 4: MTR2 Processing Parameters

Parameter	Value	Units
Processing Width	8	Inch
Processing Length	720	inch
Processing Zones*	4	#
Max Tows	6	#
Max Tow Size	50k-300k	filaments

**Each processing zone has independent control of temperature, stretch, air flow, and plasma parameters.*

Figure 46: Image of the Plasma Oxidation MTR2 in its final configuration in 2016.

Using the MTR2, it was proven that the CPIE method can be scaled economically while preserving the acceleration effect of oxidation. In addition, significant energy savings was demonstrated that will be discussed in the next chapter.

6.6 175 aMT and Larger Plasma Oxidation Oven Designs

With the MTR2 successfully demonstrated, the development work was deemed complete in the fall of 2015. The technology has now entered the commercialization phase and the design and construction has begun on a 175 aMT plasma oxidation oven. This oven will be operated to demonstrate the advantages of this technology at what industry considers a “pilot line” scale. This scale is illustrated in Figure 47. The 175 aMT will demonstrate the technology at the pilot line scale. The next step up will be full production scales of 1500 aMT and larger. This scale is shown in Figure 48.

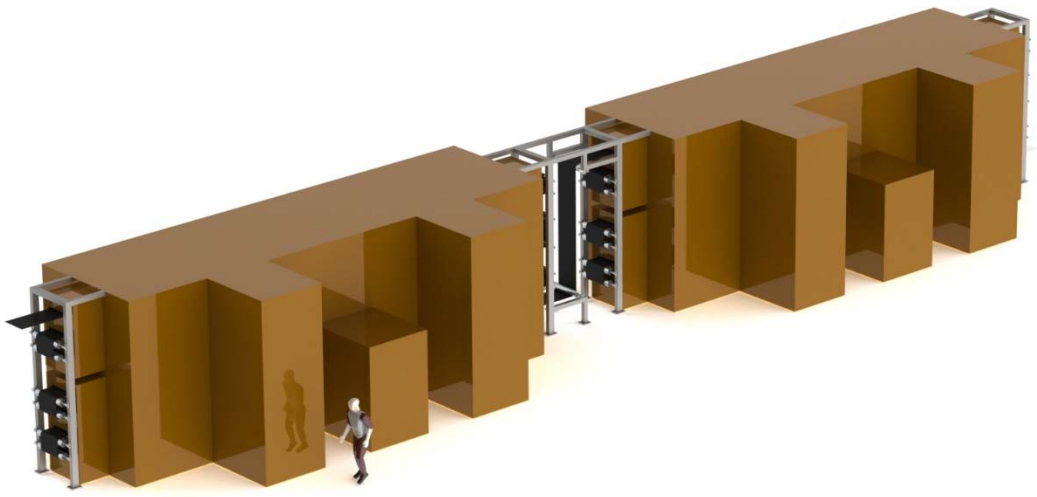

Figure 47: 175 aMT Plasma Oxidation Oven conceptual drawing.

Figure 48: Conceptual design of a 1500 annual ton plasma oxidation oven.

The critical advantages this technology can bring to the industry through the faster processing times and plasma integration is greater energy efficiency, which is a critical advantage in an energy intensive industry such as this, and much smaller equipment to deal with. Figure 49 illustrates this last point by showing a top view comparison of overall size of a plasma oxidation oven and conventional oxidation oven, both at the 1500 aMT scale.

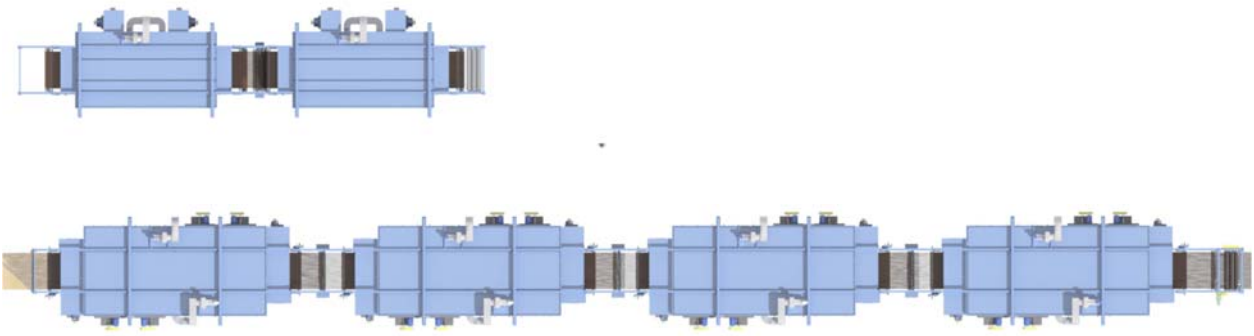

Figure 49: Comparison of a 1500 ton plasma oxidation oven (top) versus a conventional oven of the same throughput (bottom). The dot in the middle of the image is a person.

Extrapolating this size reduction to the full conversion line of equipment (which takes precursor all the way to finished carbon fiber), a full 30% reduction in length of the overall conversion line is possible when making a direct comparison, as shown in Figure 50. This simple fact will lead to reduced capital costs related to the building, utilities and installation. The next chapter will outline the publically available fiber properties obtained from this technology.

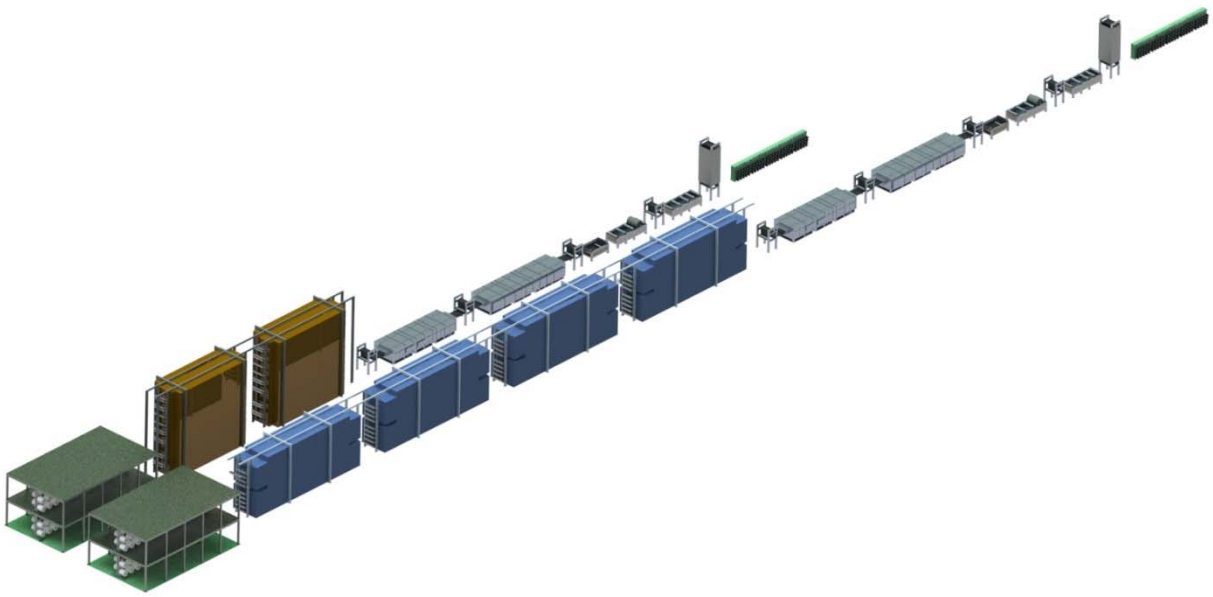

Figure 50: Comparison of a complete 1500 ton conversion line with plasma oxidation ovens (top) with a conventional conversion line of the same throughput (bottom).

CHAPTER 7: FIBER AND PERFORMANCE RESULTS

The fiber properties and equipment performance resulting from various plasma oxidation experiments presented below are from the MTR1, SMR2 and MTR2 devices previously discussed. All fiber properties are derived from single filament testing with optical microscopy measurements of diameter. Gravimetric analysis was also completed, which yielded higher mechanical values, but was only intermittently applied and so is not discussed here.

7.1 Multiple Tow Reactor 1

The MTR1 was constructed as a remote-exposure plasma oxidation oven that could process up to six small tows of precursor simultaneously. It utilized the remote plasma generator that is shown in Figure 41. This plasma generator utilized two concentric cylindrical electrodes, one of which was a column of water. This design permitted the visual observation of the plasma volume so that nonuniformities could be recognized and addressed. It generally performed well but required water-cooling and elaborate safety equipment. Its overall reliability and scalability was insufficient. Even when the plasma generator was functioning optimally, significant issues arose in its performance including poor thermal control and plasma gas distribution. In addition, to achieve sufficient density values in an accelerated timeframe, the air supply had to be supplemented with bottled oxygen, sometime to very high percentages.

It is important to note that the plasma oxidation processing only produces oxidized fiber, not carbon(ized) fiber. The most commonly accepted metric for oxidized fiber is its density. For this work, a density of 1.37 g/cc was required for the precursor being used to survive the carbonization process. Yet the amount of processing required to achieve this density was damaging the fiber. This damage was eventually reduced (bottom row), but sufficient mechanical properties could not be achieved. It was determined that the remote exposure method that was utilized with the MTR1 essentially reduces the plasma generator down to a simple ozone generator. Ozone, by itself,

does more harm than good to the precursor. The type of damage was unique and never seen before, and after considerable investigation, it was determined that excessive ozone was etching the unique indentations into the filaments. This damage is shown in Figure 51 (upper row).

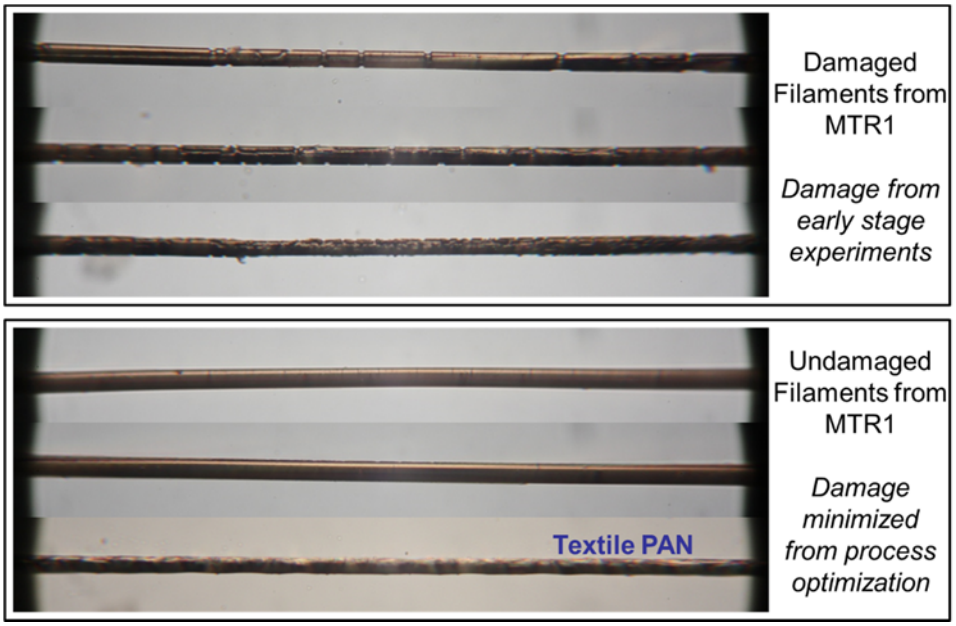

Figure 51: Images showing individual damaged filaments.

Extensive experimentation was performed using the MTR1. Test plans utilizing a combination of the Design-of-Experiments approach and "intuition-based" tests were utilized to explore the parameter space of the equipment and material involved. An example of one such test plan is shown in Table 5. In this table, parameters involving plasma power, gas flow rate, gas chemistry, processing temperature, and fiber line speed were all examined in a parametric way.[1]

[1] While line tension plays an important role in resulting fiber properties, it is not discussed here as it is considered export-controlled by the US government.

Table 5: Example test data set for MTR1.

Test	Plasma Power, W	Flow Rate, lpm	Chemistry, Air/O2	Temperature, C	Speed, in/min
1	700	20	100/0	200,200,200,200	0.5
2	700	40	80/20	200,220,225,225	0.75
3	700	60	60/40	210,240,250,250	1.0
4	950	20	100/0	200,220,225,225	0.75
5	950	40	80/20	210,240,250,250	1.0
6	950	60	60/40	200,200,200,200	0.5
7	1200	20	80/20	200,200,200,200	1.0
8	1200	40	60/40	200,220,225,225	0.5
9	1200	60	100/0	210,240,250,250	0.75
10	700	20	60/40	210,240,250,250	0.75
11	700	40	100/0	200,200,200,200	1.0
12	700	60	80/20	200,220,225,225	0.5
13	950	20	80/20	210,240,250,250	0.5
14	950	40	60/40	200,200,200,200	0.75
15	950	60	100/0	200,220,225,225	1.0
16	1200	20	60/40	200,220,225,225	1.0
17	1200	40	100/0	210,240,250,250	0.5
18	1200	60	80/20	200,200,200,200	0.75

The above test plan yielded a wide variety of results, including fiber breakage and damage. Once the fibers were oxidized in this process, they were carbonized at ORNL. For reference purposes, the Department of Energy's general minimum requirements for carbon fiber properties are shown in Table 6.

Table 6: DOE minimum program requirements and BlueStar conventional data for carbon fiber.

Parameter	DOE	Conventional
Peak Stress, ksi	250	500
Modulus, Msi	25	28
Strain, %	1	1.6

Even after months of equipment modification and refinement testing, the resulting mechanical properties for the carbonized fiber were not good.

Table 7 provides a sampling of this poor performance. The measurements made were of density, filament diameter, peak stress (tensile strength), fiber strain, and modulus (stiffness). The main reason for the poor fiber properties shown above was the plasma gas was actually damaging the fiber. Many months of work was performed to attempt to eliminate the damage being done, but the decoupling of achieving the minimum required density and the damage of the filaments was not successful. During this time, this author developed the new technique that was integrated into an existing device and yielded a solution to the damage issues.

Table 7: Selected data from MTR1 experiments. Where the sample says "Plasma Oxidized", the data is for oxidized fiber. Otherwise the data is for carbonized fiber. Additional data from the MTR1 is in the first section of Table 8 (tan rows).

Processing Date	Process	Discrete Density Gradient Column (g/cm3)	Diameter Microscopy (μm)	Peak stress (ksi)	Strain at Peak Stress (%)	Modulus (Msi)	Damage Microscopy
Test 227 Fiber from MTR1							
11/10/2009	Plasma Oxidized	1.37-1.38	12.55	17	2.92	0.6	Low/moderate
12/21/2009	Conventionally Carbonized		7.90	137.4	0.6	22.1	Low/moderate
Test 228 Fiber #1 from MTR1							
11/10/2009	SR228#1 Plasma Oxidized	1.38-1.39	13.06	26.5	5.24	1.0	Moderate
12/2/2009	Conventionally Carbonized		8.13	116.3	0.59	18.5	Moderate
12/22/2009	Conventionally Carbonized		8.53	99.8	0.51	20.0	Significant
Test 228 Fiber #2 from MTR1							
11/10/2009	SR228#2 Plasma Oxidized	1.37-1.38	N/A	N/A	N/A	N/A	Significant
12/22/2009	Conventionally Carbonized		8.82	86.4	0.46	17.2	Significant

7.2 Surface Modification Reactor 2

A completely different plasma generation and exposure technique was needed to solve the fiber damage issue. A method was devised where the plasma was integrated into the treatment chamber at the typical operating temperatures of 200 -300 ºC. This method was described in Chapter 4 and was termed the Close Proximity Indirect Exposure Method (CPIE). This process has the benefit of delivering a constant supply of short-lived reactive species to the fiber during oxidation.

Dramatic fiber property improvements were seen when progressing from the remote exposure method using the MTR1 to the close proximity indirect exposure method using the SMR2. It is important to note that, except for plasma power, which was significantly lower, the parameters that produced the results below are generally in the same range as those shown in Table 5. This data is shown in Table 8 below and is illustrated graphically in Figure 52 through Figure 54. The tan rows represent the older remote exposure results, and the blue rows show the new CPIE results. Highlighted values exceed the DOE program minimums. Not only did the transition from the remote exposure method to the close proximity indirect exposure method yield results surpassing the Department of Energy's minimums, it also produced results closer to the range of industrial grade carbon fiber (500 ksi peak stress/ 30 Msi Modulus).

In the three figures, the red dashed line represents the DOE minimum required values for each of the three properties: peak stress, modulus, and strain. The tan rows (SR374-419) are the older remote exposure data, while the blue rows (SR442-506) represents the new indirect exposure data. The graphical representation here better illustrates the dramatic improvement of the new method over the old one.

Table 8: Select fiber property data comparing the remote exposure method (tan) to the new close proximity indirect exposure method (blue).

	Oxidized						Carbonized				
Sample	Date Oxidized	Fiber Diameter (um)	Peak Stress (ksi)	Modulus (Msi)	Strain @ Break (%)	Res Time (min)	Date Carbonized	Fiber Diameter (um)	Peak Stress (ksi)	Modulus (Msi)	Strain @ Break (%)
SR374	7/9/2010	13.5	28.2	0.9	8.2	77	7/16/2010	8.59	130.0	20.3	0.61
SR376	7/12/2010	13.6	35.2	1.1	11.6	77	7/28/2010	9.3	140.1	21.2	0.65
SR381	7/16/2010	13.5	26.4	0.9	5.7	77	7/29/2010	9.4	139.8	18.7	0.73
SR408	8/13/2010	13.0	35.7	0.8	12.4	77	9/24/2010	7.78	186.0	23.2	0.75
SR415	8/20/2010	13.0	35.4	0.6	13.9	77	11/3/2010	8.84	176.8	23.9	0.74
SR419	8/27/2010	12.7	37.7	1.0	13.9	77	10/14/2010	8.96	177.8	20.9	0.83
SR442	1/18/2011	13.2	42.1	1.1	11.9	120	2/2/2011	6.95	342.5	35.6	0.93
SR460	3/8/2011	11.3	49.1	1.56	11.6	60	3/23/2011	7.2	361.2	31.7	1.09
SR466	3/14/2011	11.0	45.3	1.49	7.6	45	4/4/2011	6.99	397.5	35.5	1.07
SR472	3/22/2011	10.8	51.4	1.59	10.0	45	4/4/2011	6.95	451.6	34.9	1.20
SR473	3/23/2011	11.5	53.1	1.53	12.5	30	4/1/2011	7.62	423.9	27.7	1.39
SR478	3/28/2011	11.5	56.2	1.59	12.0	35	4/8/2011	7.5	429.7	29.0	1.38
SR485	4/12/2011	11.9	49.2	1.64	15.6	30	4/21/2011	7.12	436.2	30.5	1.30
SR488	4/14/2011	11.3	48.3	1.46	13.2	45	5/4/2011	7.11	418.9	31.4	1.25
SR489	4/14/2011	10.7	50.3	1.55	9.9	45	5/4/2011	6.51	415.8	34.8	1.11
SR491	4/18/2011	9.6	54.5	1.8	10.2	45	05/05/11	6.1	416.6	36.3	1.06
SR492	4/19/2011	11.2	46.9	1.4	13.2	45	05/05/11	7.1	358.3	32.3	1.05
SR494	4/22/2011	11.6	60.4	1.4	15.4	20	05/05/11	6.9	379.6	29.4	1.20
SR498	05/10/11	12.2	38.4	1.3	11.4	30	06/03/11	6.9	436.7	32.9	1.23
SR499	05/11/11	11.9	37.1	0.9	9.4	30	06/03/11	7.1	371.5	31.6	1.10
SR500	05/11/11	11.4	36.0	1.5	7.7	30	06/06/11	6.6	394.0	34.4	1.08
SR502	05/13/11	11.9	39.9	0.7	12.1	30	06/07/11	6.6	449.9	34.0	1.21
SR505	05/17/11	11.2	39.9	1.3	13.0	30	06/02/11	5.9	415.3	36.8	1.05
SR506	05/19/11	12.7	33.8	1.0	12.8	30	06/03/11	7.4	355.7	30.7	1.09

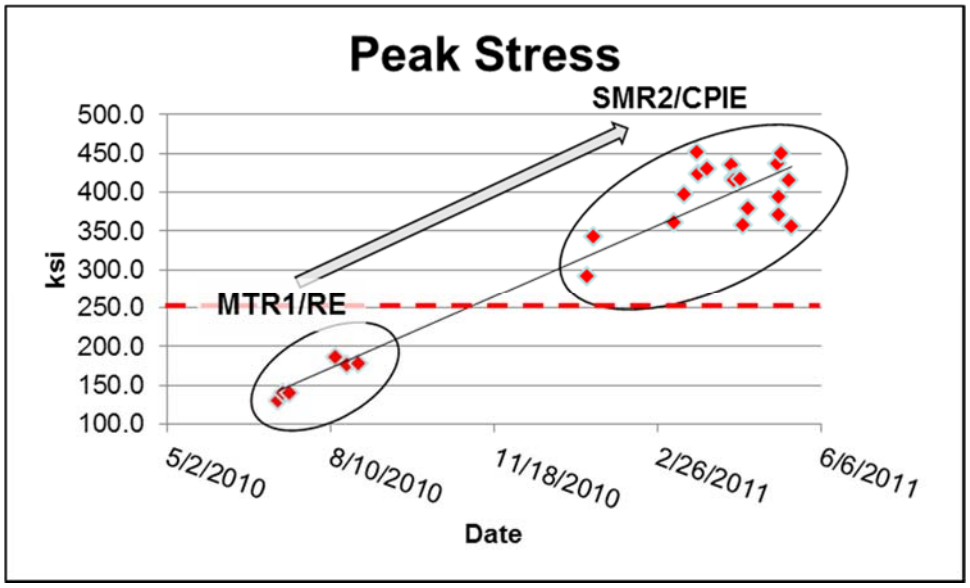

Figure 52: Chart illustrating the significant improvement in the tensile strength, or peak stress of the carbon fiber.

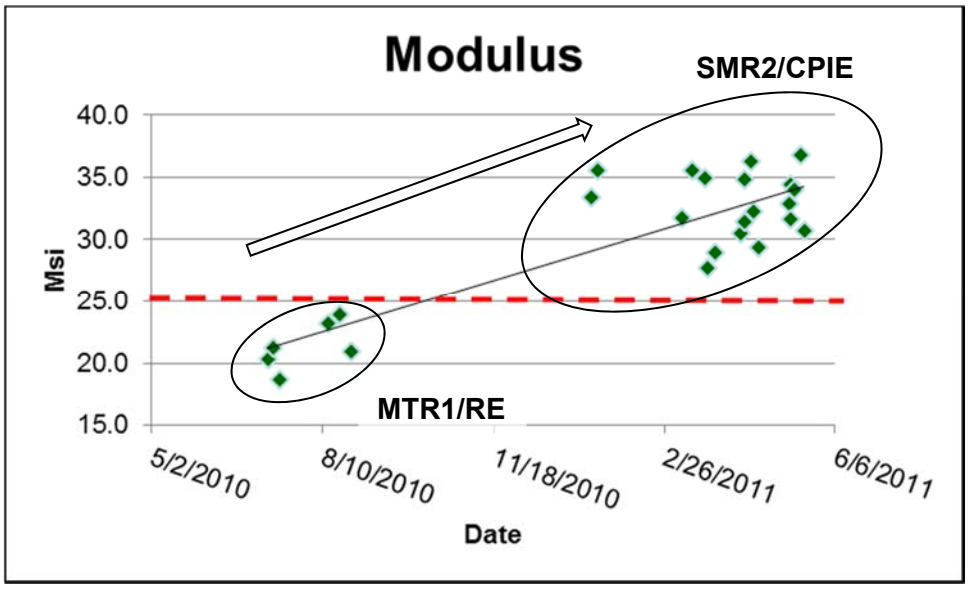

Figure 53: Chart illustrating the significant improvement in the modulus of the carbon fiber.

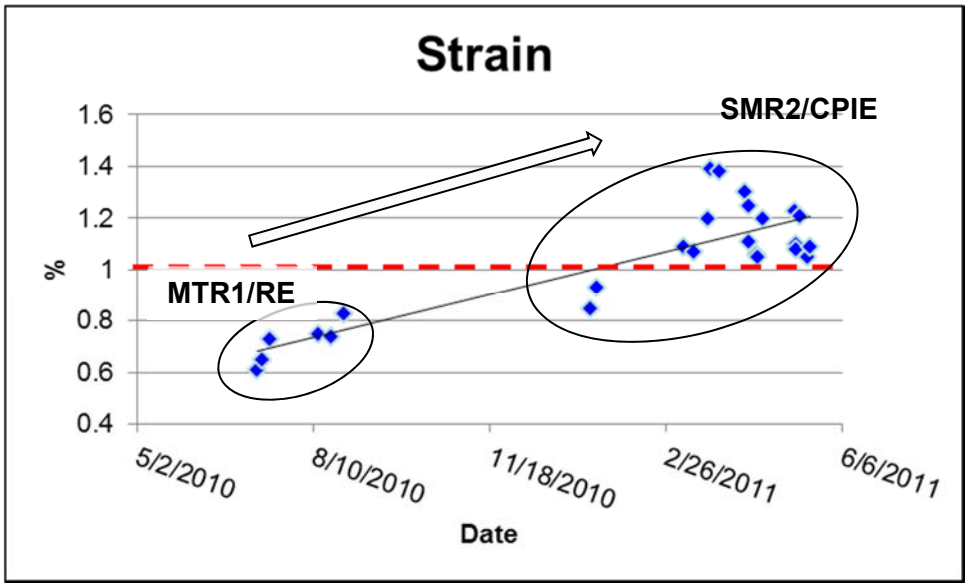

Figure 54: Chart illustrating the significant improvement in the strain of elasticity of the carbon fiber.

The new process turned out to be highly reliable, highly efficient, and highly scalable. Continued work on the SMR2 eliminated the need for the addition of oxygen to the gas stream, so simple air became the process gas. This resulted in the only utilities required for plasma oxidation were electricity and air, which are the same utilities required for conventional oxidation.

The final investigation made with the SMR2 and the new process was the process of "textile grade" PAN precursor. Textile grade precursor is acrylic fiber of quality sufficient only for textile applications with no further processing. This type of material has the same base constituent of polyacrylonitrile, but is much lower in quality and purity. The idea here was to see if plasma oxidation could improve the overall structure or performance of the fiber. Tests were conducted over several months and led to a process that could produce carbon fiber that exceeded the DOE program minimums. The oxidation processing time was 33 minutes. Normally this type of precursor would take 2 hours or more to properly oxidize. These results are shown in Figure 55 and Figure 56.

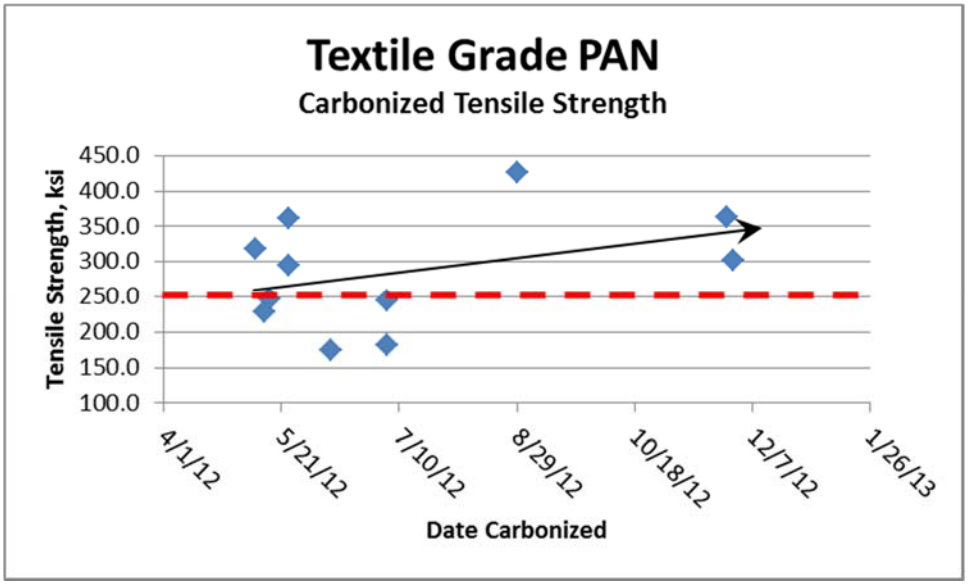

Figure 55: Tensile strength of textile grade carbon fiber that was plasma oxidized.

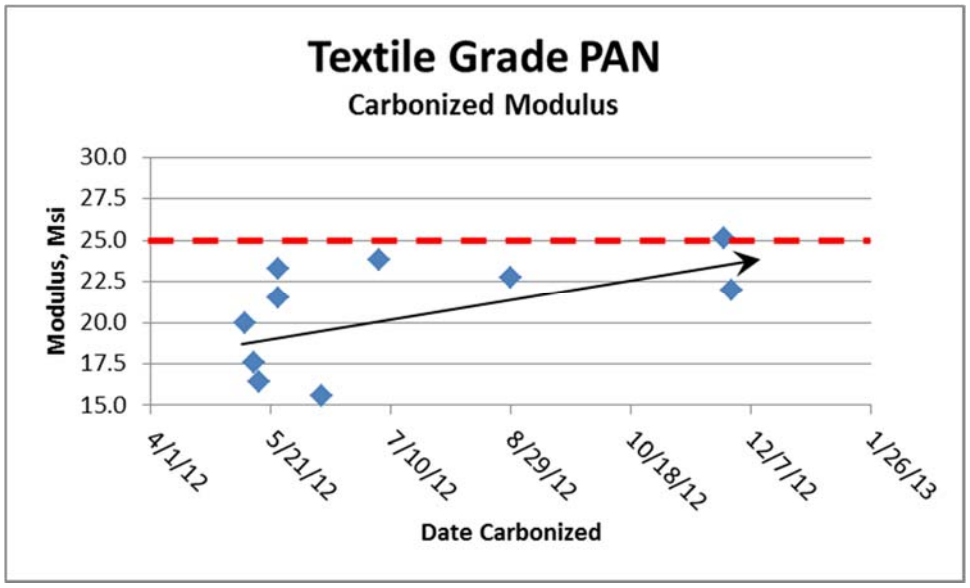

Figure 56: Modulus of textile grade carbon fiber that was plasma oxidized.

7.3 Multiple Tow Reactor 2

With the successful performance of the SMR2 demonstrated, plans were made to scale the technology to a nameplate capacity of 1 annual metric ton, or 1 aMT. While this is still very small compared to typical production levels of 1000 – 2000 aMT, it was a sufficient scale to process multiple tows of precursor in a reasonable time frame, and at an acceptable cost. This 1 aMT plasma oxidation oven was designed and constructed between 2012 and 2014, and named the Multiple Tow Reactor 2 (MTR2). Figure 57 shows the entrance of zone 1 (left) and entrance of zone 4 (right) of the MTR2 processing four tows, each with 24,000 filaments, of precursor. Notice the change in color from white to black, which is indicative of the oxidation process.

Figure 57: Multiple tows of 24,000 filament precursor being oxidized in the MTR2.

7.3.1 Fiber Properties

In 2014, a test matrix was ran over several months to examine a predetermined parameter space of tension, temperature, plasma power, airflow, and line speed for both the plasma oxidation process, and the subsequent conventional carbonization of the oxidized fibers. The results of this investigation is shown in Figure 58 for the plasma oxidized fiber, and in Figure 59 for the carbonized fiber. The results showed that the oxidized fiber properties met or exceeded the conventional values. The variation data looked at the variation of the four tows that were processed simultaneously. Samples were taken from the same lengthwise point from all four tows for a direct look at the widthwise differences in the fiber. The data showed the variation was well within expected ranges. The green dotted line represents the conventional average value projected to the plasma results for easy comparison.

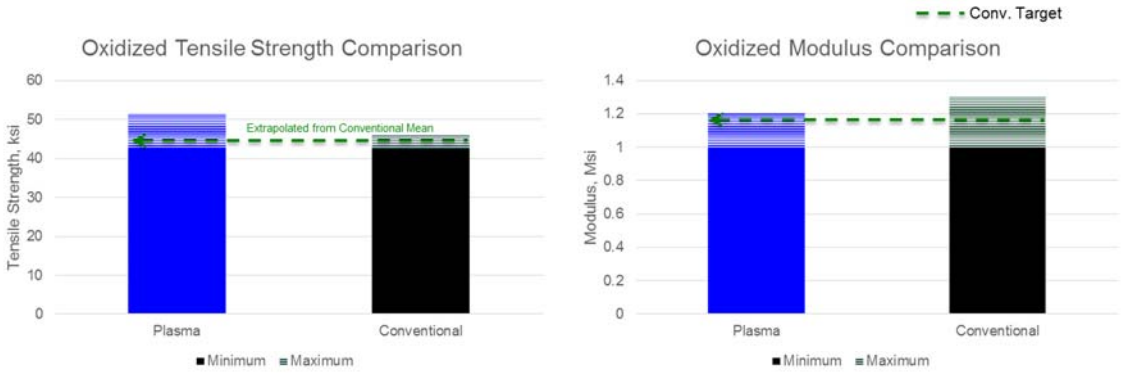

- Oxidized mechanical properties are generally equivalent to conventional.
- 4-tow plasma processing variation across tows for three stretch conditions:

Variation	Reqt.*	Cond. 1	Cond. 2	Cond. 3
Density, %	≤±3.0	+0.8/-1.1	+0.9/-1.4	+0.4/-0.4
Tensile Strength, %	≤±20	+3.5/-6.6	+6.3/-4.8	+1.1/-1.0
Modulus, %	≤±20	~0	+9.1/-9.1	~0
Strain, %	≤±20	+6.1/-6.0	+15.1/-10.1	+4.3/-8.7

Figure 58: Oxidized fiber properties from the MTR2.

Figure 59 gives the same comparison for carbonized fiber. While the modulus properties were equal or better, the tensile strength value was about 15% less than the conventional value for the best set of conditions found (the red arrows simply emphasizes the large variation in the tensile strength values due to the large number of carbonization conditions explored). The reason for this drop in tensile strength is most likely due to the lack of material sufficient to find the optimal carbonization conditions (all oxidized material was consumed during carbonization testing). The yellow dotted lines are the DOE program requirements, while the green dotted lines are the conventional values projected to the plasma results for easy comparison.

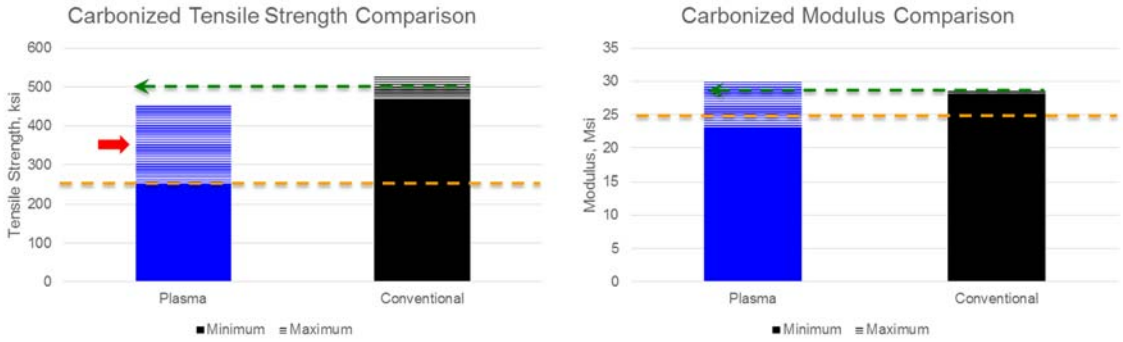

- Tensile strength is within 15% of conventional.
- Modulus is equal or better than conventional.
- 4-tow processing variation across tows for three *oxidized* stretch conditions:

Variation	Cond. 1	Cond. 2	Cond. 3
Tensile Strength, %	+4.7/-5.6	+13.0/-29.0	+16.8/-9.1
Modulus, %	+8.6/-8.8	+9.1/-17.8	+5.7/-4.3
Strain, %	+9.4/-6.2	+11.2/-13.2	+15.9/-12.1

Actual stretch conditions are not presented here.

The large variation in plasma-based tensile strength is due multiple carbonization conditions at ORNL.

Figure 59: Fiber properties of conventionally carbonized fiber that was plasma oxidized in the MTR2.

A summarized table of carbonization conditions that are shown in Figure 59 is also shown in Table 9. Here the strain values are presented as well. All values are compared with two instances of results from conventional processing (blue rows).

The final investigation made during the development work in 2015 was using 4 simultaneous tows of 48k BlueStar filaments. Here, the overall mass throughput rating of the 1 aMT plasma oxidation oven was exceeded on purpose, to test its response. The oven's maximum filament count rating was 144,000 filaments (based on 6 x 24,000 filament tows). The four 48k tows equaled 192,000 filaments, over 30% over the capacity rating. Nevertheless, the oven performed well, fully oxidizing the material in 30 minutes of heated exposure time, compared to a conventional requirement of 80 minutes. Select results are summarized in Table 10 and Table 11. Variations of the values are presented in the tables. In addition to the usual optical microscopy-based values, gravimetric-based values are presented as well. Generally, gravimetric-based values are considered more accurate. The overall values are still equal to or greater than conventional OPF mechanical values.

7.3.2 Oven Energy Performance

Another purpose of constructing and testing a plasma oxidation oven the size of the MTR2 was the ability to a) demonstrate the scalability of the CPIE approach, and b) verify the anticipated energy savings of the process. From similar testing of the above tow configurations of precursor, unit energy consumption figures were calculated. This value is in terms of kilowatt-hours (kWh) per kilogram (kg) of oxidized PAN fiber (OPF), and takes into account all major sources of power consumption from the MTR2 except for the compressed air source, which was a large compressor that is not a scalable factor. Blowers that circulated hot air in the MTR2 were included in the analysis. From reliable industry sources, a range of values from 17 – 26 kWh/kg was obtained that represent the average unit energy consumption of oxidation ovens.

Table 12 shows the results of the power measurements and energy calculations. An oxidation rate increase of 2.7X (representing a drop from a conventional 80 minutes oxidation time to 30 minutes for plasma oxidation), coupled with a more energy efficient source of heat from the plasma lead to 1 aMT number of 27 kWh/kg for 4 x 24k tows. The two "*" values of 175 aMT and 1500 aMT were obtained from an industrial scaling law obtained from a partner company. This law was used to scale the 1 aMT hard number up to production level. A final comparison can be made between the lowest conventional value of 17 kWh/kg versus the plasma oxidation number of 1.6 kWh/kg, representing a 90% energy savings.

Table 13 shows more detailed calculation results from the 4 x 48k tow testing and reveals the method involved. The total average power during the steady state range of testing is determined from the raw data stored by the LabVIEW control system. The total time of the test is recorded, and the mass throughput is calculated based on precursor properties and line speed. From the total energy and total mass, the unit energy consumption number is calculated. In addition, a "normalized" unit energy number was calculated that scales the actual number to the maximum throughput capacity of the oven. In this case, since the capacity was exceeded, the overall unit energy consumption was increased. In other cases, where the throughput is lower than the maximum, the values would increase. The purpose of this calculation was to remove the effect of mass variation and was useful for certain comparisons. In this case, even using the normalized unit energy consumption values, the energy savings compared to the 17 kWh/kg baseline was greater than 75%. The energy savings numbers were impressive, being much greater than expected values before the 1 aMT oven was made operational.

Table 9: Select samples from the carbonization of 4 x 24k plasma oxidized samples.

Sample	Density g/cc	Diameter µm	Tensile Strength ksi	Modulus Msi	Strain %
DOE Program Goal			*250*	*25*	*1*
Conventional 1	*1.80*	*7.02*	*467.3*	*28.6*	*1.48*
Conventional 2	*1.80*	*7.27*	*528.5*	*28.2*	*1.69*
MTR20075A-1	1.79	7.18	376.8	27.6	1.26
MTR20075A-3	1.78	7.15	328.4	29.8	1.04
MTR20075B-3	1.78	6.37	417.9	29.9	1.30
MTR20075C-3	1.80	7.35	402.6	25.1	1.47
MTR20077A-2	1.79	7.07	399.4	28.0	1.32
MTR20077B-1	1.78	7.43	366.9	27.5	1.24
MTR20077C-1	1.78	7.91	251.0	21.1	1.10
MTR20077D-3	1.79	6.87	396.6	26.1	1.41
MTR20078A-11	1.80	6.83	357.9	25.7	1.27
MTR20078C-5	1.79	6.64	352.5	28.4	1.16
MTR20078D-1	1.80	6.56	443.4	28.5	1.41
MTR20078D-4	1.80	6.63	453.0	26.5	1.53

Table 10: Select samples from 4 x 48k plasma oxidized samples.

SAMPLES	VALUES BASED ON OPTICAL MEASUREMENTS								VALUES BASED ON GRAVIMETRIC MEASUREMENTS				
Tow ID	Diameter by optical microscopy [µm]	*Deviation [µm]*	Peak stress [ksi]	*Deviation [ksi]*	Modulus [Msi]	*Deviation [Msi]*	Strain at peak stress [%]	*Deviation [%]*	Density Pycnom. [g/cc]	*Deviation [g/cc]*	Diameter using pycnom. [µm]	Peak stress [ksi]	Modulus [Msi]
153 A T1 (Blue Star 48k)	12.33	*1.54*	36.4	*3.9*	1.04	*0.11*	22.8	*2.9*	1.36	*0.0004*	11.42	42.4	1.21
153 B T1 (Blue Star 48k)	12.43	*1.04*	41.5	*4.8*	1.09	*0.14*	20.8	*2.3*	1.35	*0.0035*	11.27	50.5	1.33
153 C T1 (Blue Star 48k)	12.11	*1.67*	38.5	*4.8*	1.09	*0.13*	22.1	*1.7*	1.36	*0.0018*	11.32	44.1	1.25
153 D T1 (Blue Star 48k)	13.22	*0.65*	38	*3.8*	1	*0.08*	20.4	*3.4*	1.35	*0.0005*	11.30	52.0	1.37
AVERAGE	12.52	*1.23*	38.60	*4.33*	1.06	*0.12*	21.53	*2.58*	1.36		11.33	47.2	1.29
STAND. DEV.	0.48	*0.47*	2.13	*0.55*	0.04	*0.03*	1.12	*0.74*	0.01		0.06	4.7	0.07
Difference from the average to the lowest / Difference from the average to the highest (%)	-3.29% / 5.57%		-5.70% / 7.51%		-5.21% / 3.32%		-5.23% / 5.92%		-0.37% / 0.37%		-0.49% / 0.81%	-10.18% / 10.01%	-5.91% / 6.15%
MILESTONE requirements (%)	< 30		< 30		< 30		< 30		<6		< 30	< 30	< 30

Table 11: Select samples from 4 x 48k plasma oxidized samples.

SAMPLES	VALUES BASED ON OPTICAL MEASUREMENTS								VALUES BASED ON GRAVIMETRIC MEASUREMENTS				
Tow ID	Diameter by optical microscopy [µm]	*deviation [µm]*	Peak stress [ksi]	*Deviation [ksi]*	Modulus [Msi]	*Deviation [Msi]*	Strain at peak stress [%]	*Deviation [%]*	Density Pycnom. [g/cc]	*Deviation [g/cc]*	Diameter using pycnom. [µm]	Peak stress [ksi]	Modulus [Msi]
154 A T3 (Blue Star 48k)	11.92	*1.55*	38.4	*2.4*	1.33	*0.29*	21.9	*2.4*	1.3757	*0.0025*	10.91	45.9	1.59
154 B T3 (Blue Star 48k)	11.53	*0.91*	39.6	*2.8*	1.17	*0.11*	22.9	*3.8*	1.3786	*0.0022*	10.79	45.2	1.34
154 C T3 (Blue Star 48k)	12.12	*0.77*	37.5	*2.3*	1.29	*0.37*	19.8	*0.2*	1.3813	*0.001*	10.69	48.2	1.66
154 D T3 (Blue Star 48k)	12.2	*0.64*	36.8	*3.6*	1.17	*0.31*	20.4	*3.2*	1.3836	*0.0006*	10.72	47.7	1.52
AVERAGE	11.94	*0.97*	38.08	*2.78*	1.24	*0.27*	21.25	*2.40*	1.38		10.78	46.7	1.52
STAND. DEV.	0.30	*0.40*	1.21	*0.59*	0.08	*0.11*	1.41	*1.57*	0.00		0.10	1.4	0.14
Difference from the average to the lowest / Difference from the average to the highest (%)	-3.45% / 2.16%		-3.35% / 4.01%		-5.65% / 7.26%		-6.82% / 7.76%		-0.30% / 0.28%		-0.78% / 1.21%	-3.29% / 3.09%	-12.40% / 8.72%
MILESTONE requirements (%)	< 30		< 30		< 30		< 30		<6		< 30	< 30	< 30

Table 12: Unit Energy Consumption for 4x24k tows in the MTR2.

Oxidation Rate Increase	Density (g/cc)	Unit Energy Consumption (kWh/kg OPF)			Precursor
		1 aMT	175 aMT*	1500 aMT*	
2.7X	1.36	44.8	6.1	2.7	2 x 24k
2.7X	1.37	33.5	4.6	2.0	3 x 24k
2.7X	1.37	27.0	3.7	1.6	4 x 24k

Table 13: Summary of various tests of 4 x 48k tow processing in the MTR2.

Test	MTR20154 A	MTR20154 B	MTR20154 C	MTR20154 D
Average Power, W	21778.09	23044.9	21537.6	21727.8
Time, hr.	0.33	0.33	0.33	0.33
Total Energy, kWh	7.26	7.68	7.18	7.24
Input Speed, in/min	20.38	20.38	20.38	20.38
Tow Size	48000	48000	48000	48000
Tows	4	4	4	4
Linear Mass, g/in	0.74	0.74	0.74	0.74
Mass Rate, g/min	15.16	15.16	15.16	15.16
Total Mass, kg	0.30	0.30	0.30	0.30
Unit Energy, kWh/kg	23.94	25.33	23.67	23.88
Normalized Unit Energy, kWh/kg	31.92	33.77	31.57	31.84
Scaled, Normalized Unit Energy kWh/kg	3.79	4.01	3.75	3.79
Energy Savings over 17 kWh/kg	78%	76%	78%	78%

In another example of impressive energy savings, a single, large tow of over 300,000 filaments was processed in the 1 aMT oven, as shown in Figure 60 below. It is important to note that processing this large tow represented a throughput of over 200% larger than the 1 aMT oven's rated capacity. It took several weeks to arrive at stable operating conditions, but high quality OPF was produced at a 3X reduction in the conventional processing time requirement. Partly because of this high throughput capacity, the calculated unit energy consumption numbers were extremely low, as shown in Table 14 below.

With the commercialization effort underway, work continues with the 1 aMT oven to demonstrate the energy savings of the technology while the 175 aMT oven is under construction. As of the time of this writing, 6 clients have tested their precursor in the oven, with 4 more scheduled for evaluation.

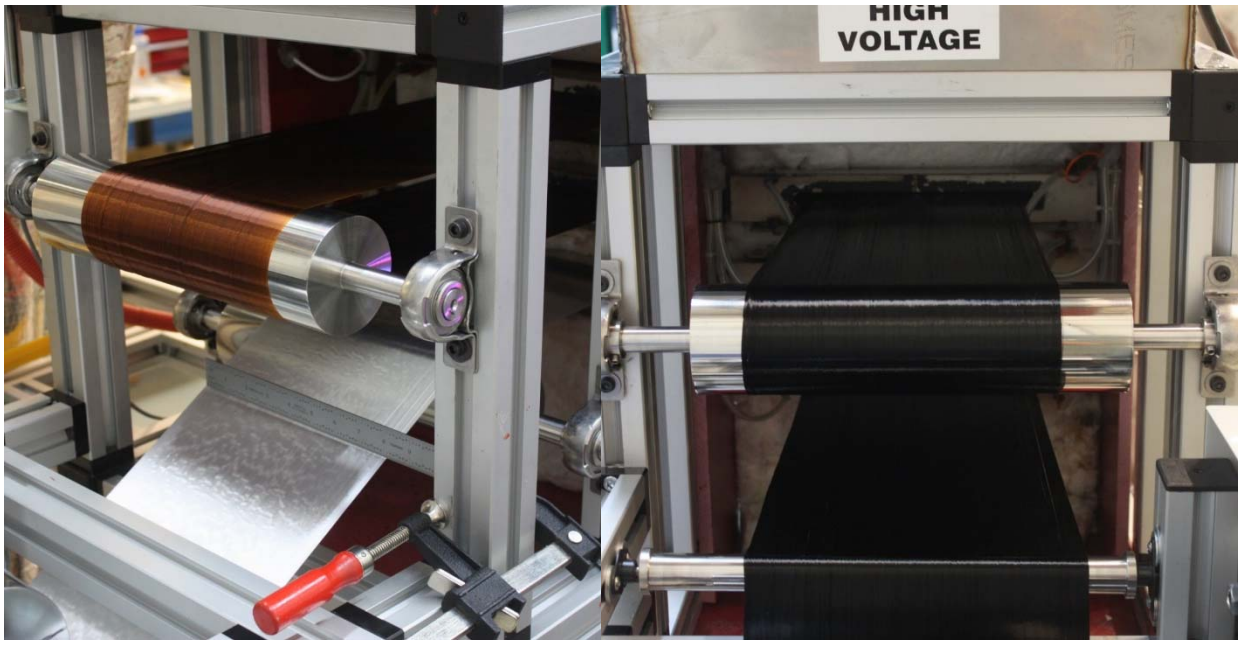

Figure 60: Large tow processing in the MTR2.

Table 14: Energy consumption for large tow processing.

Oxidation Rate Increase	Density (g/cc)	Unit Energy Consumption (kWh/kg OPF)			Precursor
		1 t/y	175 t/y*	1500 t/y*	
2.3X	1.44	10.7	1.5	0.6	~300k
3X	1.36	15.2	2.1	0.9	~150k
3X	1.38	12.3	1.7	0.7	~300k

CHAPTER 8: CONCLUSION

8.1 Final Summary

A new plasma-based method that stabilizes the carbon fiber precursor utilizing a custom designed atmospheric pressure plasma generation system has been demonstrated. Plasma based stabilization efficiently introduces oxidative reactive species that both diffuses through and react faster with the precursor filaments, resulting in a faster and more efficient process. This was a brand new process never before attempted and led to new performance standards for this particular step of the carbon fiber manufacturing process. A robust theory was presented that described the plasma oxidation mechanism. Different control techniques were discussed, and the hardware evolution and implementation was presented. Finally, fiber properties and equipment performance was presented. The equipment was ultimately scaled to the 1 aMT scale which is sufficient to demonstrate the technology and produce significant amount of material for subsequent processing and analysis. Using the 1 aMT plasma oxidation oven, it was verified that the oxidation process was accelerated 2.5-3X over the conventional baseline, reduced unit energy consumption by over 75%, all while producing carbon fiber with properties that met or exceeded conventional standards.

8.2 Future Work

This technology is currently being scaled from the 1 aMT level to 175 aMT. While this is occurring the opportunity exists to conduct a more thorough examination of the relationship between process conditions and final fiber properties with the goal of building a systems-based model that could be used with more advanced control techniques. In addition, once the 175 aMT oven is operational, that scale of operations will allow for more detailed analysis of off-gassing from the fiber during processing to judge the impact on the efficiency of the plasma chemistry effect, and to determine if there are beneficial effects on the hazardous chemistry that is exhausted out of

the oven and routed to treatment devices. Also, with the 175 aMT oven, sufficient processing data could be generated to create more advanced modeling for simulation work. It is anticipated that the current design and process will be continually advanced over time.

REFERENCES

[1] A. Fridman and L. A. Kennedy, *Plasma Physics and Engineering*. New York: Taylor & Francis, 2004.

[2] A. Otto, *Space Weather: The Physics Behind a Slogan*. Springer Science & Business Media, 2005.

[3] J. R. Roth, *Industrial Plasma Engineering. Volume 1: Principles*. Bristol: Institute Of Physics Publishing, 1995.

[4] C. Red, "2015 Global Markets for Carbon Fiber Composites: Adaptations to High Growth and Market Maturity," in *Carbon Fiber Conference*, 2015.

[5] O. P. Bahl, Z. Shen, J. G. Lavin, and R. A. Ross, "Manufacture of Carbon Fibers," in *Carbon Fibers*, 3rd ed., J.-B. Donnet, T. K. Wang, J. C. M. Peng, and S. Rebouillat, Eds. New York: Marcel Dekker, Inc., 1998, pp. 1–84.

[6] F. Paulauskas, "Advanced Oxidation & Stabilization of PAN-Based Carbon Precursor Fibers," in *Department of Energy Annual Merit Review*, 2015.

[7] U. Kogelschatz, "Dielectric-Barrier Discharges: Their History, Discharge Physics, and Industrial Applications," *Plasma Chem. Plasma Process.*, vol. 23, no. 1, 2003.

[8] K. H. Becker, U. Kogelschatz, K. H. Schoenbach, and R. J. Barker, Eds., "Non-Equilibrium Air Plasmas at Atmospheric Pressure," in *Non-Equilibrium Air Plasmas at Atmospheric Pressure*, Bristol: Institute Of Physics Publishing, 2005.

[9] J. R. Roth, *Industrial Plasma Engineering. Volume 2: Applications to Nonthermal Plasma Processing*. Bristol: Institute Of Physics Publishing, 2001.

[10] L. S. Polak, G. B. Sinyarev, D. I. Slovetskii, A. A. Ovsyannikov, Y. A. Lebedev, G. K. Vinogradov, F. B. Vurzel', V. F. Nazarov, and A. A. Levitskii, *Plasma Chemistry*. Cambridge: Cambridge International Science Publishing, 1998.

[11] M. Vardelle, A. Vardelle, P. Fauchais, and M. I. Boulos, "Plasma - Particle Momentum and Heat Transfer: Modelling and Measurements," *Am. Inst. Chem. Eng. J.*, vol. 29, no. 2, pp. 236–243, 1983.

[12] D. Orlov, T. Corke, and M. Patel, "Electric circuit model for aerodynamic plasma actuator," in *AIAA Aerospace Sciences Meeting and Exhibit*, 2006, no. January, pp. 9–12.

[13] S. Kurniawan, D. J. Djoko Satjojo H. S., and S. P Sakti, "Voltage-Current Measurement and Circuit Model Simulation to Characterize Electrical Properties of 40 kHz Capacitive Coupled Plasma (CCP) By Means of Pressure Variation," *Appl. Phys. Res.*, vol. 8, no. 2, p. 10, 2016.

[14] A. Flores-Fuentes, R. Pena-Eguiluz, R. Lopez-Callejas, A. Mercado-Cabrera, R. Valencia-Alvarado, S. Barocio-Delgado, and A. de la Piedad-Beneitez, "Electrical Model of an Atmospheric Pressure Dielectric Barrier Discharge Cell," *IEEE Trans. Plasma Sci.*, vol. 37, no. 1, pp. 128–134, 2009.

[15] A. Fridman, A. Chirokov, and A. Gutsol, "Non-thermal atmospheric pressure discharges," *J. Phys. D. Appl. Phys.*, vol. 38, no. 2, p. R1, 2005.

[16] D. Gidon, D. B. Graves, and A. Mesbah, "Model predictive control of thermal effects of an atmospheric pressure plasma jet for biomedical applications," *Am. Control Conf.*, pp. 4889–4894, 2016.

[17] M. P. Patel, Z. H. Sowle, T. C. Corke, and C. A. He, “Autonomous sensing and control of wing stall using a smart plasma slat,” *J. Aircr.*, vol. 44, no. 2, pp. 516–527, 2007.

[18] L. Peebles, *Carbon Fibers*. Boca Raton: CRC Press, 1995.

[19] P. Morgan, *Carbon Fibers and Their Composites*. Boca Raton: Taylor & Francis, 2005.

[20] F. Paulauskas, “Advanced Oxidation & Stabilization of PAN-Based Carbon Precursor Fibers,” Washington, DC, 2012.

[21] X. Huang, “Fabrication and properties of carbon fibers,” *Materials (Basel).*, vol. 2, no. 4, pp. 2369–2403, 2009.

[22] J. Delmonte, “Surface Treatment of Carbon/Graphite Fibers,” in *Technology of Carbon and Graphite Fiber Components*, 1981, pp. 189–191.

[23] H. Thomas, “Founded on the invention of Corona Treatment,” 2012. [Online]. Available: http://www.vetaphone.com/founded-on-the-invention-of-corona-treatment/.

[24] F. Paulauskas and D. M. Sherman, “Apparatus and method for stabilization or oxidation of polymeric materials,” US7649078, 2005.

[25] F. Paulauskas, D. M. Sherman, and T. L. White, “Apparatus and method for oxidation and stabilization of polymeric materials,” US7534854, 2005.

[26] F. Paulauskas, D. M. Sherman, and T. L. White, “Apparatus and method for oxidation and stabilization of polymeric materials,” US7786253, 2005.

[27] G. E. Georghiou, a P. Papadakis, R. Morrow, and a C. Metaxas, “Numerical modelling of atmospheric pressure gas discharges leading to plasma production,” *J. Phys. D. Appl. Phys.*, vol. 38, pp. R303–R328, 2005.

[28] Y. V Serdyuk, a Larsson, S. M. Gubanski, and M. Akyuz, “The propagation of positive streamers in a weak and uniform background electric field,” *J. Phys. D. Appl. Phys.*, vol. 34, no. 4, pp. 614–623, 2001.

[29] H. Nishida, T. Nonomura, and T. Abe, “Characterization of Electrohydrodynamic Force on Dielectric-Barrier-Discharge Plasma Actuator Using Fluid Simulation,” *World Acad. Sci. Eng. Technol.*, vol. 71, no. November, pp. 321–325, 2012.

[30] N. Benard, A. Debien, and E. Moreau, “Time-dependent volume force produced by a non-thermal plasma actuator from experimental velocity field,” *J. Phys. D. Appl. Phys.*, vol. 46, no. 24, p. 245201, 2013.

[31] T. Hurtig, A. Larsson, and M. Liefvendahl, “Electrohydrodynamic Flow Control - A literature Survey,” 2007.

[32] J. P. Boeuf, Y. Lagmich, T. Unfer, T. Callegari, and L. C. Pitchford, “Electrohydrodynamic force in dielectric barrier discharge plasma actuators,” *J. Phys. D. Appl. Phys.*, vol. 40, no. 3, pp. 652–662, 2007.

[33] C. L. Enloe, R. S. Mangina, and G. I. Font, “Normalized Electronegative Species Effects in the Dielectric-Barrier-Discharge Plasma Actuator,” *AIAA J.*, vol. 54, no. 7, pp. 1–8, 2016.

[34] J. P. Boeuf, Y. Lagmich, and L. C. Pitchford, “Contribution of positive and negative ions to the electrohydrodynamic force in a dielectric barrier discharge plasma actuator operating in air,” *J. Appl. Phys.*, vol. 106, p. 23115, 2009.

[35] R. Schiffman, *Handbook of Industrial Drying*, 3rd ed. Boca Raton: Taylor & Francis Group, 2007.

[36] B. Eliasson and U. Kogelschatz, “N2O Formation in Ozonizers,” *J. Chim. Phys. physico-chimie Biol.*, vol. 83, no. 4, pp. 279–282, 1986.

[37] I. Plante, “Energetic and chemical reactivity of atomic and molecular oxygen,” 2010.

[38] J. J. Lowke and R. Morrow, “Theoretical Analysis of Removal of Oxides of Sulphur and Nitrogen in Pulsed Operation of Electrostatic Precipitators,” *IEEE Trans. Plasma Sci.*, vol. 23, no. 4, pp. 661–671, 1995.

[39] J. T. Herron and D. S. Green, “Chemical kinetics database and predictive schemes for nonthermal humid air plasma chemistry. Part II. Neutral species reactions,” *Plasma Chem. Plasma Process.*, vol. 21, no. 3, pp. 459–481, 2001.

[40] I. Introduction, “Parametric Study of Particle Size for Plasma Actuator PIV,” *52nd Aerosp. Sci. Meet.*, no. January, pp. 1–10, 2014.

[41] G. E. Morfill and A. V. Ivlev, “Complex plasmas: An interdisciplinary research field,” *Rev. Mod. Phys.*, vol. 81, no. 4, pp. 1353–1404, 2009.

[42] R. Dorf and R. Bishop, *Modern Control Systems*, 8th ed. Addison Wesley Longman, Inc., 1998.

[43] J. G. Ziegler and N. B. Nichols, “Optimum Settings for Automatic Controllers,” *Trans. A.S.M.E*, vol. 64, pp. 759–768, 1942.

[44] F. Paulauskas, A. Naskar, and T. Bonds, “Advanced Oxidation Method for Producing High-Density Oxidized Polyacrylonitrile Fibers,” 14715831, 2015.

[45] F. Paulauskas and T. A. Bonds, “Atmospheric pressure plasma processing of polymeric materials utilizing close proximity indirect exposure,” US9447205, 2012.

[46] T. Bonds, “Plasma Oxidation of Carbon Fiber Precursor,” in *CAMX Conference Proceedings*, 2016.

[47] “R&D100 Award Finalists,” 2016. [Online]. Available: http://www.rd100conference.com/awards/winners-finalists/6416/plasma-oxidation-oven-rapid-low-energy-polymer-oxidation/. [Accessed: 03-Oct-2016].

VITA

Truman Bonds was born in Maryville, TN, to the parents of Richard and Sandra Bonds. He is the middle child with two sisters, Sarah and Rebekah. He attended Heritage High School in Maryville, TN. After graduation, he decided to pursue electrical engineering at the University of Tennessee, Knoxville. He obtained a Bachelors of Science degree in 2000 in Electrical Engineering. He then began working full-time at the university in instructional technology while pursuing a graduate degree. He obtained a graduate research assistantship in 2004 in the Plasma Sciences Laboratory under Dr. Reece Roth. He obtained a Masters of Science degree in Electrical Engineering, with a concentration on plasma engineering in 2006. In 2011 he co-founded RMX Technologies, LLC to begin commercialization of plasma technologies he helped develop in conjunction with the Oak Ridge National Laboratory. He is continuing his education with a PhD in Electrical Engineering at the University of Tennessee, Knoxville and expects to obtain this in 2016.